AD_____

Award Number: DAMD17-00-1-0352

TITLE: Regulation of Tumor Progression by Mgat5-Dependent Glycosylation

PRINCIPAL INVESTIGATOR: Dr. James W. Dennis

CONTRACTING ORGANIZATION: Samuel Lunenfeld Research Institute of Mount Sinai Hospital
Toronto, Ontario, Canada M5G 1X5

REPORT DATE: July 2001

TYPE OF REPORT: Annual

PREPARED FOR: U.S. Army Medical Research and Materiel Command
Fort Detrick, Maryland 21702-5012

REPORT DOCUMENTATION PAGE

Form Approved
OMB No. 074-0188

1. AGENCY USE ONLY (Leave blank)	2. REPORT DATE	3. REPORT TYPE AND DATES COVERED
	July 2001	Annual (1 Jun 00 - 1 Jun 01)

4. TITLE AND SUBTITLE
Regulation of Tumor Progression by Mgat5-Dependent Glycosylation

5. FUNDING NUMBERS
DAMD17-00-1-0352

6. AUTHOR(S)
Dr. James W. Dennis

7. PERFORMING ORGANIZATION NAME(S) AND ADDRESS(ES)
Samuel Lunenfeld Research Institute
of Mount Sinai Hospital
Toronto, Ontario, Canada M5G 1X5

E-Mail: Dennis @MSHRI.on.ca

8. PERFORMING ORGANIZATION REPORT NUMBER

9. SPONSORING / MONITORING AGENCY NAME(S) AND ADDRESS(ES)
U.S. Army Medical Research and Materiel Command
Fort Detrick, Maryland 21702-5012

10. SPONSORING / MONITORING AGENCY REPORT NUMBER

11. SUPPLEMENTARY NOTES
Report contains color

12a. DISTRIBUTION / AVAILABILITY STATEMENT
Approved for Public Release; Distribution Unlimited

12b. DISTRIBUTION CODE

13. Abstract *(Maximum 200 Words)* *(abstract should contain no proprietary or confidential information)*

Task 1 was to further define the phenotype of *Mgat5*$^{-/-}$ cells regarding adhesion, signal transduction, and growth factor responsiveness. We have established immortalized embryonic fibroblast cell lines form Mgat5-/- mice, made Mgat5 retrovial vector for rescue of the mutant phenotypes, and established new technology (the Cellomics scan array system) to measure these parameters with precision. **Task 2** was to use genetic methods to analysis *Mgat5* dependent tumor progression *in vivo*. We have interbred Mgat5 mice with Pten mutant mice and preliminary results suggest the genes interaction, in the immune system and cancer. **Task 3&4** was to location β1,6GlcNAc-branched N-glycans that mediate phenotype. We identified T cell receptor and a new mechanism of N-glycan action, and more will identified this year.

14. Subject Terms (keywords previously assigned to proposal abstract or terms which apply to this award)
Protein glycosylation. glvcosyltransferase, cell adhesion, cadherins, integrins, cytokine receptors

15. NUMBER OF PAGES
43

16. PRICE CODE

17. SECURITY CLASSIFICATION OF REPORT	18. SECURITY CLASSIFICATION OF THIS PAGE	19. SECURITY CLASSIFICATION OF ABSTRACT	20. LIMITATION OF ABSTRACT
Unclassified	Unclassified	Unclassified	Unlimited

Table of Contents

INTRODUCTION:

Cancer-associated changes in glycoprotein glycosylation are well-documented (1), but the molecular functions of these carbohydrates in disease progression are poorly understood. GlcNAc-TV (Golgi β1-6N-acetylglucosaminyltransferase V) is highly expressed in proliferating and migrating cells, and the *Mgat5* gene is transcribed in response to activation of the RAS/MAPK/ETS pathway. The enzyme is required during the post-translational modification of glycoproteins with β1-6GlcNAc-branched asparagine-linked oligosaccharides (N-glycans). Adhesion receptors involved in tumor progression including $\alpha_1\beta_5$ integrin, E-cadherins and CD44 are suggested to have these glycans. To examine the function of GlcNAc-TV dependent glycosylation, we have generated mice deficient in this enzyme by targeted mutation of the *Mgat5* locus. *Mgat5*$^{-/-}$ mice were viable, fertile and lacked β1,6GlcNAc-branched N-glycans. The *Mgat5*$^{-/-}$ mice were crossed with transgenic mice expressing the polyomavirus middle T oncogene under the control of the mouse mammary tumor virus long terminal repeat (MMTV-PyMT) (2). Breast carcinomas in GlcNAc-TV deficient mice developed with longer latency, tumors grew more slowly, and the incidence of lung metastases was reduced by >90%. Focal adhesion formation, cell spreading and PKB phosphorylation was impaired in *Mgat5*$^{-/-}$ fibroblasts. Membrane ruffling was reduced in MMTV-PyMT tumor cells. These observations suggest the Mgat5 deficiency suppresses focal adhesion turnover and PI3 kinase (PI3K) activation. Consistent with this, *Mgat5*$^{-/-}$ leukocyte show impaired migration *in vivo*, and enhanced adhesion to fibronectin. The Mgat5$^{-/-}$ mice displayed increased susceptibility to autoimmune disease, and we have demonstrated this year that the N-glycans bind to galectins, which regulate T cell receptor clustering in response to agonist (3). This mechanism of action may also regulate clustering of other receptors such as the integrins and cadherins, an hypothesis currently being tested within the mandate of this grant.

Our studies on the *Mgat5*$^{-/-}$ mice suggest that Mgat5-dependent glycosylation may regulate multiple receptors by altering their response to extracellular ligands. Our working **hypothesis** is that cancer-associated increases in GlcNAc-TV-dependent glycosylation can be initiated via the RAS pathways, which enhances focal adhesion signaling via PI3K/PKB, and promotes cell motility, tumor growth and metastasis. Genetic manipulations in cell culture and in mice will be done to identify signaling proteins and pathways that are dependent upon Mgat5 glycosylation. The research is intended to define the effects of *Mgat5*$^{-/-}$ mutation on membrane ruffling, and activation of focal adhesion signaling in cell culture. Further, to use genetic methods and identify downstream effectors of Mgat5 by interbreeding mice with mutations that may interact in an epistatic or synergy manner regarding the cancer and immune phenotypes. We will determine the location of β1,6 branched N-glycans on specific glycoproteins by mass spectrometry, and where possible, their effects on glycoprotein function in isolation. At this time, integrins $\alpha_1\beta_5$, E-cadherin and CD44 are candidates, but others will be identified and characterized in the course of these studies.

By identifying molecular interactions between Mgat5-modified glycans and adhesion receptors and their intracellular signaling pathways, a rational for combination therapies that includes carbohydrate-processing inhibitors (CPI) will be developed. Although CPIs targeting Mgat5 may be effective at slowing tumor progression and

metastasis, combination therapies are more likely to meet the challenge posed by multiple overlapping oncogenic pathways.

BODY:

The research in the first year has been focussed on defining a working model for Mgat5-modified N-glycans regulation of receptor signaling with T cell receptor and integrins as the models (3; 4).

Task 1 was to further define the phenotype of *Mgat5*$^{-/-}$ cells regarding adhesion, signal transduction, and growth factor responsiveness. We have established that most PyMT-induced mammary tumors in *Mgat5*$^{-/-}$ mice grow slowly, and displayed impaired focal adhesion signaling and PI3K/PKB activation (2). Approximately 5% of the tumor progressed to fast growth, and these tumors regained full PI3K/PKB signaling. These results further support the effect of Mgat5 as a positive regulator of focal adhesion signaling that collaborates with PyMT oncogene to stimulate growth and survival of tumor cells via the PI3K/PKB pathway.

We have established immortalized *Mgat5*$^{-/-}$ embryonic fibroblast cell lines as well as tumor cell lines as required in task 1 to study adhesion migration and signal transduction. We have also designed and constructed a Mgat5 retroviral vector, to transfect cells *Mgat5*$^{-/-}$ cells and demonstrate phenotypic rescue, as required to confirm the mutant phenotypes, notably cell adhesion, migration, and signal transduction. Our research institute acquired new technology in May 2001 to measure cell migration, spreading, and nuclear translocation of activated proteins in signaling cascades. The Cellomics Scan Array is an automated fluorescence microscope with software to measure and quantify multiple cellular parameter on individual cells (5). The instrument is designed for high through put analysis in 96 well plates and will be ideal for completion of task 1 experiments.

To validate and test the assays for cytoplasmic-nuclear translocation of signaling proteins, we began by used anti-Smad2 antibodies to measure TGF-β1 dependent Smad2 nuclear translocation and inhibition by an antagonist (Ahsg/fetuin) (Figure 1,2). After 15 min of TGF-β1 treatment, the distribution of Smad-2 protein in the nucleus and cytoplasm shows a shift into the nucleus, which was doses dependent (Figure 1). Ahsg inhibition was also does dependent (Figure 2). Ras- mediated induction of P38 and Erk nuclear translocation, as well as PKB/Akt induced translocation of FKH is underway. We will generate data for *Mgat5*$^{-/-}$ cells as well as cells with the combined mutation of Mgat5$^{-/-}$ and Pten$^{+/-}$ (see below). Cellomics Inc has promised delivery of software for cell spreading and migration this month, which will allow us to rapidly complete the objectives in task with better qualitative methods than originally anticipated. With the new methods, there has been some delay in completing task 1, but we believe this is work while, as the Cellomics methods will be more accurate.

We will also test carbohydrate-processing inhibitors in combinations with drugs that that interer with the Ras and PI3K pathways using the Cellomics assays as per our original task outline.

Task 2: We are using genetic methods to analysis *Mgat5*-dependent tumor progression *in vivo*. We have interbred Mgat5 mice with Pten mutant mice and preliminary results suggest these genes interaction, in the immune system and cancer.

Pten is a 3-inositol PI3 phosphatase, a negative regulator of the PKB/Akt pathway, and of focal adhesion signaling and invasion (6-9), a pathway very commonly mutated in many human cancer (10; 11). $Pten^{+/-}$ mice also show an inflammatory autoimmune disease and a high incidence of tumors in breast, lymphomas and other organs. In preliminary experiments, we have observed that some abnormalities in splenic T cell distribution in the single mutant mice mice are normalized in the $Mgat5^{-/-}$;$Pten^{+/-}$ double mutant mice (Figure 3).

We have examined the effect of Mgat5 on PyMT breast cancer induction on F2 mice of 129/sv x FVB mice, and on 129/sv. The results demonstrate that the strains differ for expression of a modifier gene that governs the potency of the $Mgat5^{-/-}$ anti-tumor effects. Analysis of strain-specific SNPs and gene expression profiling will be done on tail and tumor samples, respectively in the second year, as originally planned. The cancer phenotypes of Mgat5 on FVB and 129 backgrounds appear to be sufficiently distinct, and therefore, we should be able to map genes and their strain-specific alleles that are causal in the cancer phenotype. This should reveal genes that interact with Mgat5 to enhance or inhibit its effects in cancer growth and progression in vivo.

Task 3: We are attempting to identify targets for Mgat5 glycosylation that are important in cancer growth. We have identified T cell receptor as a target for Mgat5-dependent regulation, and depletion of Mgat5 enhances immune sensitivity, a possible anti-cancer mechanism. In addition, we have determined the Mgat5-glycans interact with galectins at the cell surface. The interaction forms a lattice of glycoproteins that impedes receptor clustering. This is a novel mechanism of action for glycan regulation of signaling receptors, and we will determine whether a similar mechanism regulates adhesion receptors. The Mgat5 glycans on substratum adhesion receptors and their interaction with galectins may be serve to destabilize adhesion plaques and accelerate turnover and promote cell migration.

Task 4 was to location β1,6GlcNAc-branched N-glycans that mediate phenotype. We identified T cell receptor and a new mechanism of N-glycan action, and more will identified this year. If the analysis of E-cadherin confirms the presence of Mgat5 glycans, we will examine the functionality of the glycoforms in cell adhesion assays as originally outlined.

KEY RESEARCH ACCOMPLISHMENTS:

- We have established $Mgat5^{-/-}$ fibroblast and breast tumor cell lines in preparation for the functional studies in task 1. A Mgat5 rescuing retroviral vector is ready to use.
- We have tested a new assay for analysis of cell signaling and motility, the Cellomics scan array, which will ultimate speed the completion of task 1.
- We have determined that Mgat5 glycosylation regulates T cell receptor clustering and immune sensitivity in vivo, an important new mechanistic understanding.
- We have generated Mgat5 crosses with Pten mutant mice, and preliminary results suggest gene interactions that must be confirmed at the biochemical level.
- The Mgat5 effects on tumor growth are subject to modifier gene(s) that differ in 129/sv and FVB mouse strains. This gene(s) will be mapped by SNP analysis and tumors characterized by gene chip analysis.

REPORTABLE OUTCOMES:

- Publications:

We published a key paper this year in the high-impact journal ***Nature*** and a paper in press describing the wider implications of our findings in ***Current Opinions in Structural Biology.***

- Patent:

A US patent application was files coving methods of drug discovery based on the concept of N-glycans as a modifier of receptor clustering.

- Invited Lectures:

Dr. Dennis has presented aspects of this work at Gordon Conference on Glycobiology, Ventura CA, and the International Symposium on Protein Traffic, Interlaken, Switzerland. Invited lecture at NIH immunology Group on Aug 6th. Dr. Demetriou presented at the Keystone conference on Regulation of Immunity and Autoimmunity.

- Trainees:

Mike Demetriou MD, PhD
Pam Chueng, a Ph.D. student in the Molecular and Medical Genetics Department at University of Toronto has been working on project since early 2000.
Joby McKenzie will join this Sept as a PhD student.

CONCLUSIONS: The generation of cell lines, mouse strains, and new methods required to complete the tasks were the major focus of the work in the last year. With most of these materials in hand, we will complete the tasks as outlined with only minor modifications in methodology. We published 3 key papers in the last year and discovered an important new mechanism of action for Mgat5 glycans regulation of signaling receptor using the T cell receptor as the model. We are in an excellent position to complete the project tasks, and make a significant contribution to our understanding of breast cancer progression and treatment.

REFERENCES:

1. Hakomori, S.-I. Aberrant glycosylation in tumors and tumor-associated carbohydrate antigens. Adv.Cancer Res., *52*: 257-331, 1989.

2. Granovsky, M., Fata, J., Pawling, J., Muller, W.J., Khokha, R., and Dennis, J.W. Suppression of tumor growth and metastasis in Mgat5-deficient mice. Nature Med., *6*: 306-312, 2000.

3. Demetriou, M., Granovsky, M., Quaggin, S., and Dennis, J.W. Negative regulation of T-cell activation and autoimmunity by Mgat5 N-glycosylation. Nature, *409*: 733-739, 2001.

4. Dennis, J.W., Warren, C.E., Demetriou, M., and Granovsky, M. Genetic defects in *N*-glycosylation and cellular diversity in mammals. Curr.Opin.Struct.Biol., *in press*: 2001.

5. Taylor, D.L., Woo, E.S., and Giuliano, K.A. Real-time molecular and cellular analysis: the new frontier of drug discovery. Curr Opin Biotechnol, *1*: 75-81, 2001.

6. Gu, J., Tamura, M., and Yamada, K.M. Tumor suppressor PTEN inhibits integrin- and growth factor-mediated mitogen-activated protein (MAP) kinase signaling pathways. J.Cell Biol., *143*: 1375-1383, 1998.

7. Stambolic, V., Suzuki, A., de la Pompa, J.L., Brothers, G.M., Mirtsos, C., Sasaki, T., Ruland, J., Penninger, J.M., Siderovski, D.P., and Mak, T.W. Negative regulation of PKB/Akt-dependent cell survival by the tumor suppressor PTEN. Cell, *95*: 29-39, 1998.

8. Tamura, M., Gu, J., Matsumoto, K., Aota, S., Parsons, R., and Yamada, K.M. Inhibition of cell migration, spreading, and focal adhesions by tumor suppressor PTEN. Science, *280*: 1614-1617, 1998.

9. Maier, D., Jones, G., Li, X., Schonthal, A.H., Gratzl, O., Van Meir, E.G., and Merlo, A. The PTEN lipid phosphatase domain is not required to inhibit invasion of glioma cells. Cancer Res., *59*: 5479-5482, 1999.

10. Marsh, D.J., Dahia, P.L., Caron, S., Kum, J.B., Frayling, I.M., Tomlinson, I.P., Hughes, K.S., Eeles, R.A., Hodgson, S.V., Murday, V.A., Houlston, R., and Eng, C. Germline PTEN mutations in Cowden syndrome-like families. J.Med.Genet., *35*: 881-885, 1998.

11. Li, J., Yen, C., Liaw, D., Podsypanina, K., Bose, S., Wang, S.I., Puc, J., Miliaresis, C., Rodgers, L., McCombie, R., Bigner, S.H., Giovanella, B.C., Ittmann, M., Tycko, B., Hibshoosh, H., Wigler, M.H., and Parsons, R. *PTEN*, a putative protein tyrosine phosphatase gene mutated in human brain, breast, and prostate cancer. Science, *275*: 1943-1947, 1997.

APPENDICES:

Granovsky, M., Fata, J., Pawling, J., Muller, W.J., Khokha, R., and Dennis, J.W. Suppression of tumor growth and metastasis in Mgat5-deficient mice. Nature Med., *6*: 306-312, 2000.

M. Demetriou, M. Granovsky, S. Quaggin J. W. Dennis. Negative regulation of T cell receptor and autoimmunity by *Mgat5* N-glycosylation. **Nature** 409:733-739, (2001).

J.W. Dennis, C.E. Warren and M. Demetriou M. Granovsky. Genetic defects in *N*-glycosylation and cellular plasticity in mammals. **Current Opinions** in press (2001)

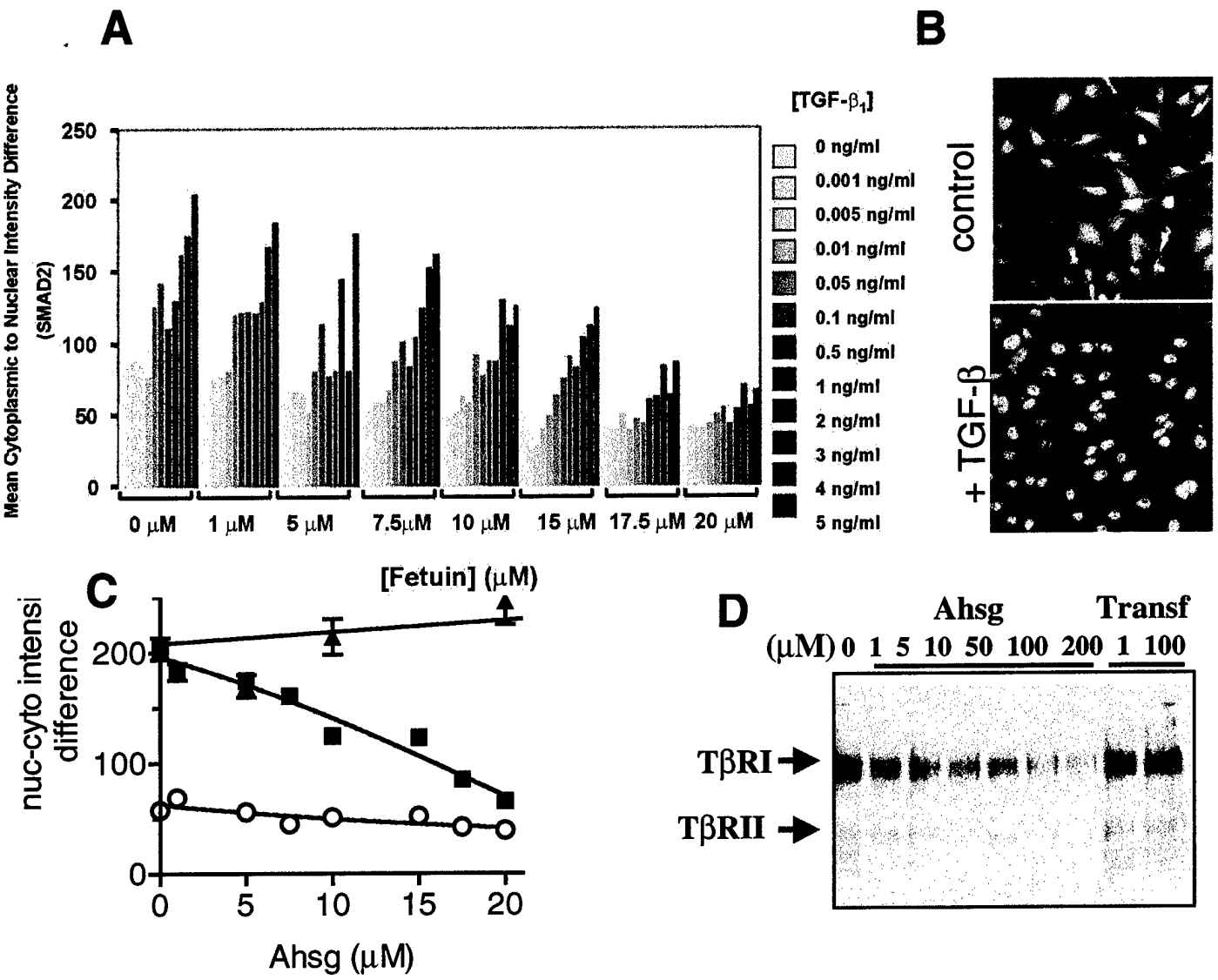

Pilot study demonstrating signal transduction by cytoplasmic-nuclear translocation of Smad2 using the Cellomics Scan Array. (A) Mink lung epithelial cell were stimulated with various doses of TGF-β1 in the presence of increasing concentrations of the antagonist Ahsg, using a 2-D array in a 96 well plate. The cells were fixed 15 minutes later and stained with mouse anti-Smad-2 antibodies, plus a fluorescent labeled 2nd antibody. Each bar represents cyto-nuclear differences averaged for 100 cells measured in each of the 96 well. (B) Cellomics images. (C) A summary of Ashg (squares) and transferrin (triangles) TGF-β antagonist activity at highest concentration of TGF-β1 (200 nM), or using Ahsg alone (circles). (D) A demonstration of Ahsg competition for ^{125}I-labeled TGF-β1 binding to cell surface receptors. The right 2 lanes are controls with transferrin.

Figure 1

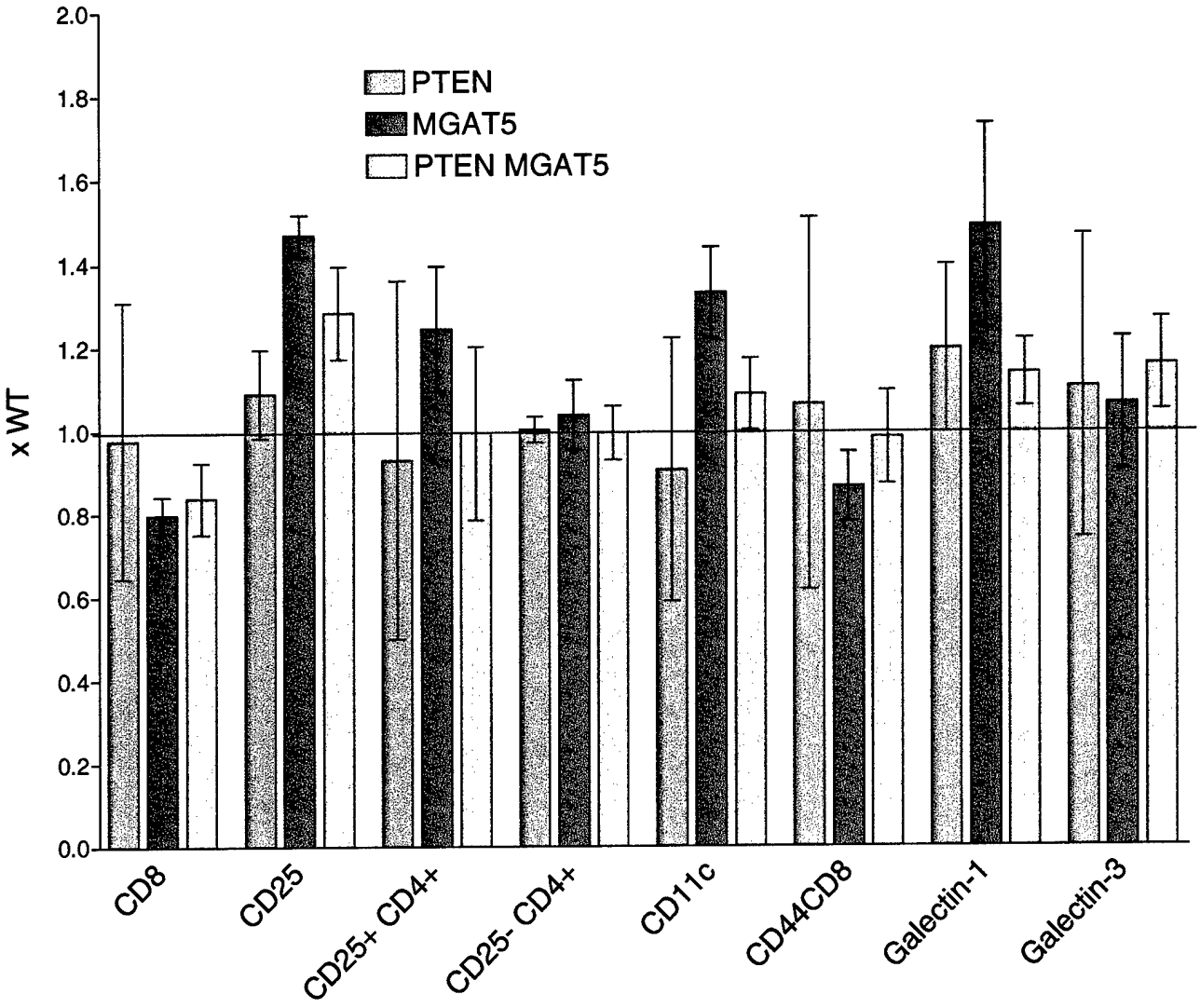

FACS analysis of spleen cells for various CD markers using 5 mice per genotype ($Mgat5^{-/-}Pten^{+/-}$; $Mgat5^{+/+}Pten^{+/-}$; $Mgat5^{-/-}Pten^{+/+}$; $Mgat5^{+/+}Pten^{+/+}$. The fraction of positive cells was normalized to wild type mice ($Mgat5^{+/+}Pten^{+/+}$) for this representation. Note that the double mutant tends towards normalization for the CD25, CD11c and galectin-1. The variance seen in Pten+/- is also reduced in the double mutants.

Figure 2

Suppression of tumor growth and metastasis in Mgat5-deficient mice

MARIA GRANOVSKY[1,2], JIMMIE FATA[3], JUDY PAWLING[1], WILLIAM J. MULLER[4], RAMA KHOKHA[3] & JAMES W. DENNIS[1,2]

[1]*Samuel Lunenfeld Research Institute, Mount Sinai Hospital 600 University Ave. R988, Toronto, Ontario, Canada M5G 1X5*
[2]*Department of Molecular & Medical Genetics, University of Toronto, Toronto, Ontario, Canada*
[3]*Department of Medical Biophysics, University of Toronto, Ontario Cancer Institute, Princess Margaret Hospital, 620 University Ave., Toronto, Ontario, Canada M5G 2C1*
[4]*Institute for Molecular Biology and Biotechnology, McMaster University, Hamilton, Ontario, Canada L8S 4K1*
Correspondences should be addressed to: J.W.D.; email: Dennis@mshri.on.ca

Golgi β1,6N-acetylglucosaminyltransferase V (MGAT5) is required in the biosynthesis of β1,6GlcNAc-branched N-linked glycans attached to cell surface and secreted glycoproteins. Amounts of MGAT5 glycan products are commonly increased in malignancies, and correlate with disease progression. To study the functions of these N-glycans in development and disease, we generated mice deficient in Mgat5 by targeted gene mutation. These *Mgat5*$^{-/-}$ mice lacked Mgat5 products and appeared normal, but differed in their responses to certain extrinsic conditions. Mammary tumor growth and metastases induced by the polyomavirus middle T oncogene was considerably less in *Mgat5*$^{-/-}$ mice than in transgenic littermates expressing Mgat5. Furthermore, Mgat5 glycan products stimulated membrane ruffling and phosphatidylinositol 3 kinase–protein kinase B activation, fueling a positive feedback loop that amplified oncogene signaling and tumor growth *in vivo*. Our results indicate that inhibitors of MGAT5 might be useful in the treatment of malignancies by targeting their dependency on focal adhesion signaling for growth and metastasis.

Malignant transformation is accompanied by increased β1,6GlcNAc-branching of N-glycans attached to Asn-X-Ser/Thr sequences in mature glycoproteins[1,2]. The β1,6GlcNAc-branched N-glycans are tri (2,2,6)- and tetra (2,4,2,6)-antenna-like oligosaccharides that constitute a subset of the 'complex-type' N-glycans (Fig. 1*a*). The medial Golgi enzyme β1,6N-acetylglucosaminyltransferase V (MGAT5 (mannoside acetyl glucosaminyl transferase 5) or GlcNAc-TV) catalyzes the addition of β1,6-linked GlcNAc and defines this subset of N-glycans[3,4] (Fig. 1*a*). The plant lectin leukoagglutinin (L-PHA) binds specifically to mature MGAT5 products (Fig. 1*a*)(ref. 5). L-PHA has been used to measure these N-glycans in tissue sections (Fig. 1*b* and ref. 6). MGAT5 products in breast and colorectal carcinomas correlate with poor prognosis and decreased survival time[6,7].

MGAT5 enzyme activity increases in fibroblast and epithelial cell lines with expression of the oncogenes *v-src*, T24-*H-ras* and *v-fps*, and in cells infected with polyomavirus or rous sarcoma virus[2,8,9,10]. Transcription of the *MGAT5* gene is positively regulated by signaling downstream of these oncogenes, notably by the Ras–Raf–Ets pathway[11,12]. Studies on transplantable tumors in mice have indicated that Mgat5 products contribute directly to the cancer growth and metastasis. For example, somatic tumor cell mutants deficient in Mgat5 activity produce fewer spontaneous metastases and tumors grow slower than wild-type cells[10,13]. In addition, forced expression of Mgat5 in epithelial cells results in loss of contact inhibition, increased cell motility, morphological transformation in culture, tumor formation in athymic nude mice[14], and enhanced metastasis[15].

MGAT5 selectively substitutes only a subset of N-glycan intermediates, presumably specified by the structural features of the glycoprotein substrates[16]. Structural analysis of glycans on specific glycoproteins remains incomplete, but has shown that MGAT5 products are present on the integrins LFA-1 and $\alpha_1\beta_5$ (refs. 17,18). The amount of MGAT5 product on integrin subunits α_5, α_v and β_1 increase in cells transfected with *MGAT5*, and the cells show increased motility and decreased substratum adhesion[14]. The larger size of MGAT5 products may impede or alter the kinetics of protein–protein interactions that mediate cell–cell and cell–substratum adhesion. Indeed, large N-glycans present on CD44 (ref. 19), intracellular adhesion molecule-1 (ref. 20) and CD43 (ref. 21) decrease the ligand-binding activity of these cell adhesion receptors, although the *in vivo* importance of these observations has been unclear.

Here, we generated Mgat5-deficient mice by targeted gene mutation in embryonic stem (ES) cells to assess the function of Mgat5 products in normal development and cancer progression. Activating mutations in *Ras* genes, as well as mutations leading to activation of protein kinase B (PKB; also known as Akt) are commonly found in human tumors[22,23]. The *Polyomavirus* middle T antigen (PyMT) viral oncogene activates these pathways[24,25], which together contribute to transformation and multifocal tumors in mice expressing PyMT from a transgene in mammary epithelium[26–29]. Here, PyMT-induced tumor growth and metastasis were considerably suppressed in Mgat5-deficient mice compared with that in their PyMT-transgenic littermates expressing Mgat5. Moreover, *Mgat5* gene expression was induced by the

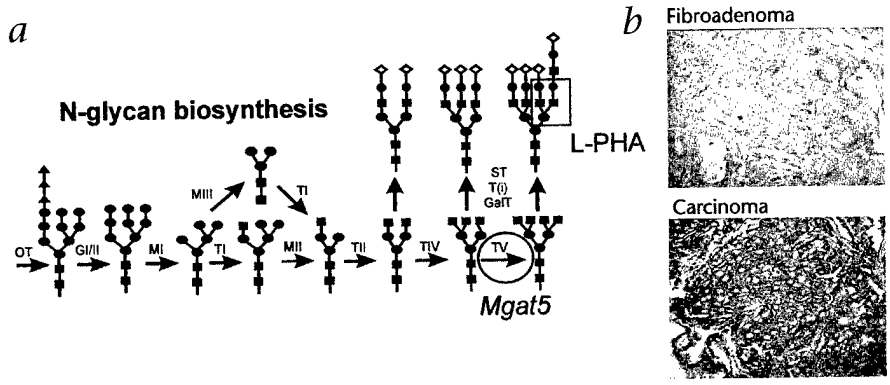

Fig. 1 MGAT5 in N-glycan biosynthesis, and overexpression of its products in human cancers. ***a***, Golgi N-glycan biosynthesis pathway, showing MGAT5 (TV) in the production of a tetra (2,4,2,6)-antenna-like oligosaccharide (numbers in brackets represent linkages of the 'antennae', left to right). OT, oligosaccharyltransferase; GI and GII, the α-glucosidases; TI, TII, TIV, TV T(i), the β-N-acetylglycosaminyltransferases; MI, the α1,2mannosidases; MII, MIII, α1,3/6mannosidases; Gal-T, β1,4-galactosyltransferases; ST, α-sialyltransferases. The boxed structure Galβ1,4GlcNAcβ1,6(Galβ1,4GlcNAcβ1,2)Manα binds L-PHA (ref. 5). ***b***, L-PHA lectin histochemical staining of a human benign fibroadenoma and breast carcinoma using steptoavidin–horseradish peroxidase for detection as described[6].

PyMT oncogene. Finally, the products of Mgat5 promoted focal adhesion turnover, which amplified PyMT-dependent activation of phosphatidylinositol 3 (PI3) kinase–PKB, and promoted tumor growth and metastasis.

Mgat5$^{-/-}$ mice are viable and lack Mgat5 products

We designed the *Mgat5* targeting vector to replace the coding portion of the first exon of *Mgat5* with the *lacZ* reporter gene (Fig. 2*a* and *b*). We isolated two independent homologous recombinant ES clones and injected them into blastocytes to produce chimeric mice. Alleles from both ES cell lines were successfully transmitted from chimeric mice to progeny. *Mgat5*$^{-/-}$ mice were generated from heterozygous parents with a normal frequency of 25%. We determined the *Mgat5* genotypes of the mice by Southern blot analysis (Fig. 2*b*) and by PCR analysis (data not shown). Mgat5 enzyme activity was approximately 50% in heterozygous mice, and below the level of detection in *Mgat5*$^{-/-}$ mice (Fig. 2*c* and *d*). We did not detect Mgat5 products in *Mgat5*$^{-/-}$ tissues by L-PHA lectin probing of western blots, indicating that mutation of the *Mgat5* locus had eliminated essentially all catalytic activity and Mgat5 products in the *Mgat5*$^{-/-}$ mice (Fig. 2*e*). Mgat5-deficient mice developed normally, producing normal numbers of pups, but adult *Mgat5*$^{-/-}$ mice had several phenotypic abnormalities, including leukocyte recruitment into inflamed tissues, an age-related decrease in the cellularity of kidney glomerulli, an apparent deficiency in nurturing behavior, and T-cell hypersensitivity to T-cell receptor agonists. These phenotypes are now being analyzed. Peripheral white cell and erythrocyte counts were normal, and populations of T and B cells in spleen, thymus and lymph nodes were also in the normal range, as assessed by fluorescence-activated cell sorting analysis (data not shown). There was no weight loss or premature mortality in the *Mgat5*$^{-/-}$ mice up to 18 months of age.

LacZ activity in *Mgat5*$^{+/-}$ embryos was distributed like that of *Mgat5* transcripts (Fig. 3*a* and *b*), indicating the reporter gene faithfully reflected *Mgat5* transcription in mouse tissues[30]. LacZ activity, *Mgat5* transcripts and L-PHA reactivity also co-localized in adult tissues. In the cerebellum, the neuronal cell bodies stained for lacZ and the neural dendritic trees stained with L-PHA; the latter is consistent with localization of glycoproteins to plasma membrane and secretory compartments (Fig. 3*c* and *d*). Therefore, lacZ activity in mice with *Mgat5*-mutant alleles could be used to monitor *Mgat5* promoter activity *in vivo*.

Cancer growth and metastasis are reduced in *Mgat5*$^{-/-}$ mice

We crossed PyMT-transgenic mice with *Mgat5*-mutant mice and measured tumor latency, tumor growth and the incidence of lung metastases in the progeny. We first detected mammary tumors in PyMT *Mgat5*$^{+/-}$ and PyMT *Mgat5*$^{+/+}$ female mice at 8 weeks of age, and by 16 weeks 50% of the mammary pads had tumors (Fig. 4*a* and *b*). In contrast, 50% tumor incidence in the PyMT *Mgat5*$^{-/-}$ mice occurred at 24 weeks, and by 27 weeks of age, tumors were detected in all mammary fat pads. PyMT *Mgat5*$^{+/+}$ male

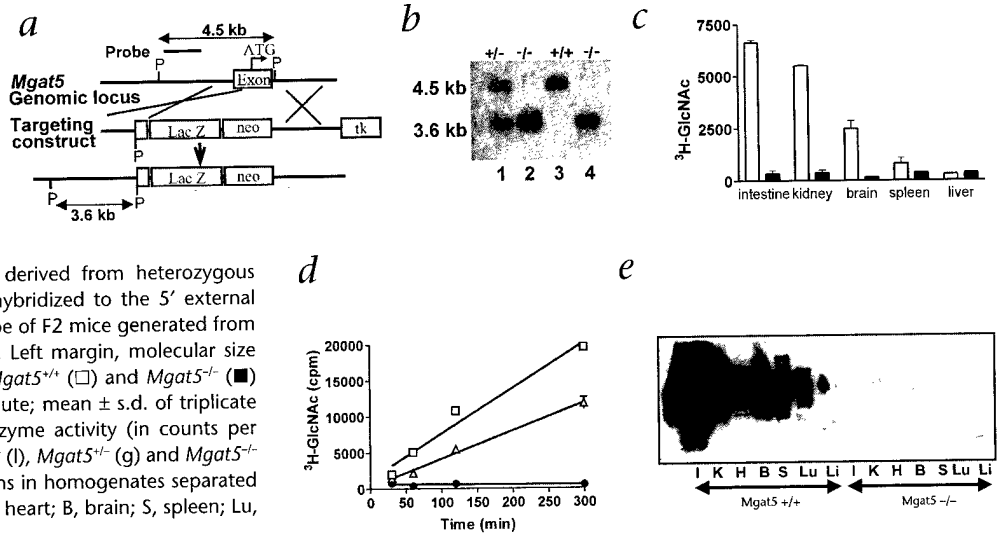

Fig. 2 Targeted mutation of the *Mgat5* locus in mice. ***a*** and ***b***, The wild-type *Mgat5* locus, the targeting vector, and the resulting targeted locus. Nucleotides –22 to 241 of the first coding exon were replaced with *lacZ* and a neomycin-resistant gene. ▩, exon; ■ (above *Mgat5* genomic locus), 5′ external probe; P, *Pst*I restriction site. *b*, Southern blot analysis of genomic DNA of F2 offspring derived from heterozygous crosses. DNA digested with *Pst*I was hybridized to the 5′ external probe. Lanes 2 and 4, *Mgat5*$^{-/-}$ genotype of F2 mice generated from two independently targeted ES clones. Left margin, molecular size markers ***c***, Mgat5 enzyme activity in *Mgat5*$^{+/+}$ (□) and *Mgat5*$^{-/-}$ (■) tissue homogenates (in counts per minute; mean ± s.d. of triplicate samples).***d***, Time course of Mgat5 enzyme activity (in counts per minute) in small intestine from *Mgat5*$^{+/+}$ (l), *Mgat5*$^{+/-}$ (g) and *Mgat5*$^{-/-}$ (P) mice. ***e***, L-PHA-reactive glycoproteins in homogenates separated by SDS–PAGE. I, intestine; K, kidney; H, heart; B, brain; S, spleen; Lu, lung; Li, liver.

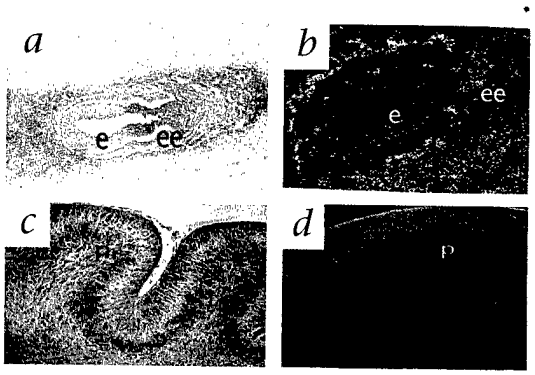

Fig. 3 Mouse embryo at embryonic day 7.5. ***a*** and ***b***, Section through the center of embryo. *a*, lacZ expression, visualized by X-gal staining (blue). *b*, Darkfield microscopy, showing *Mgat5* transcripts detected by RNA *in situ* hybridization. ***c*** and ***d***, Cerebella of mice at postnatal day 6. *LacZ* expression from the targeted *Mgat5* allele corresponds to L-PHA staining. The neuronal cell bodies stain for *lacZ* (*c*) and the neural dendritic trees stain with L-PHA (*d*); the latter is consistent with localization of glycoproteins to plasma membrane and secretory compartments. t, trophoblasts; e, embryonic tissue; ee, extraembryonic tissue; p, Purkinje cells.

mice developed tumors between 6 and 9 months and tumor development in *Mgat5*$^{-/-}$ male mice was delayed until 10–13 months (data not shown). Tumors in PyMT *Mgat5*$^{-/-}$ mice grew more slowly than those in heterozygous and wild-type mice (Fig. 4*c*). At 28–30 weeks of age, the tumor burden in PyMT *Mgat5*$^{-/-}$ mice was 3.4 ± 0.8 g, compared with 15.1 ± 1.8 g and 13 ± 2.8 g in the PyMT *Mgat5*$^{+/-}$ and PyMT *Mgat5*$^{+/+}$ mice, respectively. The fraction of cells staining positive for proliferating cell nuclear antigen was substantially less in PyMT *Mgat5*$^{-/-}$ neoplastic and carcinoma tissues than in similar tissues in PyMT *Mgat5*$^{+/-}$ mice (Fig. 4*d*). The frequency of apoptotic cells in the tumors was 1–2% and did not vary substantially with *Mgat5* genotype (data not shown). Northern blot analysis indicated that PyMT transcript amounts were similar in tumors from the three *Mgat5* genotypes (data not shown).

The incidence of lung metastases in PyMT *Mgat5*$^{-/-}$ mice was about 5% that in wild-type and heterozygous littermates (Fig. 4*e*). The metastatic tumor nodules in lung were smaller in the PyMT *Mgat5*$^{-/-}$ mice, and tumor burden in the lung did not cause cardiac hypertrophy (0 of 15 mice), which was common in the PyMT *Mgat5*$^{+/+}$ and PyMT *Mgat5*$^{-/+}$ mice at late stages of tumor growth (13 of 27 mice).

Before overt tumor formation, the branching morphology of ductal epithelium was similar in PyMT *Mgat5*$^{-/-}$ and PyMT *Mgat5*$^{+/-}$ mice (Fig. 5*a* and *b*). In mammary fat pads lacking overt tumors at 14 weeks, there were multiple microscopic tumor foci in mice of all *Mgat5* genotypes. This indicates that although tumor growth was considerably less, multiple focal initiation was not suppressed in Mgat5-deficient mice. At 26 weeks, tumors in *Mgat5*$^{+/-}$ and *Mgat5*$^{+/+}$ PyMT-transgenic mice had completely replaced the ductal epithelium, whereas mammary fat pads from PyMT *Mgat5*$^{-/-}$ mice contained areas of normal tissue, hyperplasia and neoplasia (Fig. 5*c* and *d*).

LacZ activity was absent in normal and hyperplastic mammary tissues of PyMT *Mgat5*$^{+/-}$ and PyMT *Mgat5*$^{-/-}$ mice (Fig. 5*e*). PyMT *Mgat5*$^{-/-}$ tumors expressed small amounts of *LacZ* activity with some foci of intensely staining tumor cells, whereas PyMT *Mgat5*$^{+/-}$ tumors stained strongly. We found that 5 of 140 tumors in PyMT *Mgat5*$^{-/-}$ mice had acquired a fast-growth phenotype, similar to tumors in transgenic mice expressing Mgat5. These tumors, which had escaped growth suppression dependent on *Mgat5*$^{-/-}$, also expressed more *lacZ* activity (Fig. 5*f* and *g*). This indicates that the *Mgat5* promoter was activated in concert with the molecular event(s) leading to a fast-growth phenotype. L-PHA-reactive N-glycans were not re-expressed in the fast-growing PyMT *Mgat5*$^{-/-}$ tumors (data not shown).

Mgat5$^{-/-}$ stabilizes focal adhesions and actin stress fibers

Overexpression of MGAT5 in cultured epithelial cells blocks contact inhibition of growth, and cell–substratum adhesion on collagen and fibronectin[14]. Therefore, we removed mammary tumor cells from PyMT-transgenic mice and cultured them on fibronectin-coated cover slips in serum-free medium to assess cell spreading, microfilament organization and focal adhesions. PyMT *Mgat5*$^{-/-}$ tumor cells showed impaired membrane ruffling compared with that of PyMT *Mgat5*$^{+/+}$ cells. The former cells showed actin stress fiber networks with paxillin in a punctate distribution of focal adhesions beneath the cells, whereas paxillin in the PyMT *Mgat5*$^{+/-}$ cells was very concentrated in ruffled

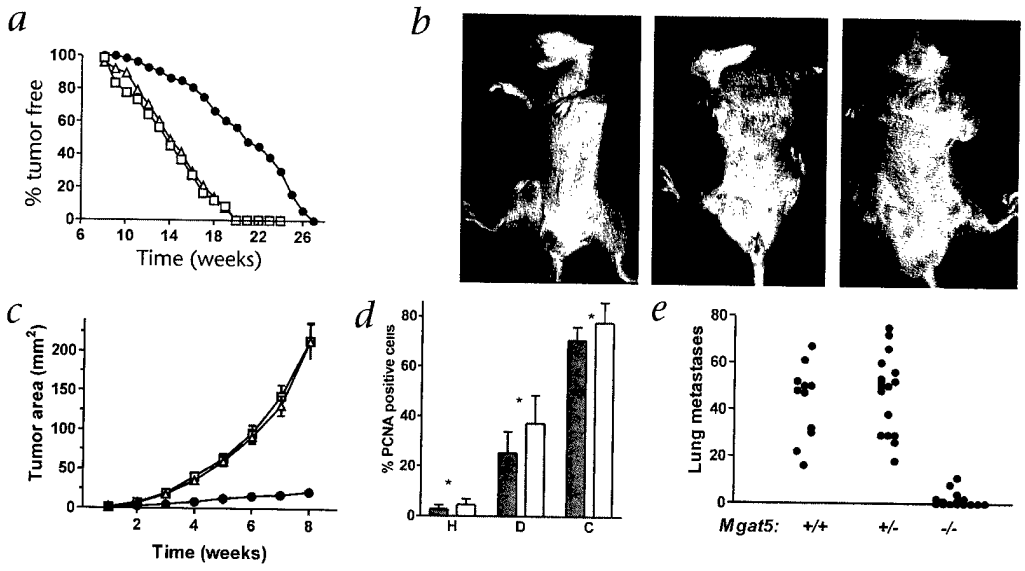

Fig. 4 PyMT-dependent tumor growth is suppresses in *Mgat5*$^{-/-}$ mice. ***a***, Fraction of mammary pads free of palpable tumors in PyMT-transgenic littermates with either *Mgat5*$^{+/+}$ (□; $n = 9$), *Mgat5*$^{+/-}$ (△; $n = 17$) or *Mgat5*$^{-/-}$ (●; $n = 14$) genotypes. ***b***, PyMT-transgenic mice at 26 weeks of age. ***c***, Tumor growth (omitting the 5 of 140 fast-growing tumors), plotted as mean tumor surface area ± s.e.m.; time 0, initial detection by palpation. ***d***, Sections of mammary fat pad from *Mgat5*$^{-/-}$ (■) and *Mgat5*$^{+/+}$ (□), stained with antibodies against proliferating cell nuclear antigen to quantify the proliferating cell fraction in hyperplasia (H), dysplastia (D) and carcinoma (C). ***e***, Incidence of lung metastases per mouse at 24–30 weeks of age, when mammary tumor burden necessitated killing of the mice expressing Mgat5.

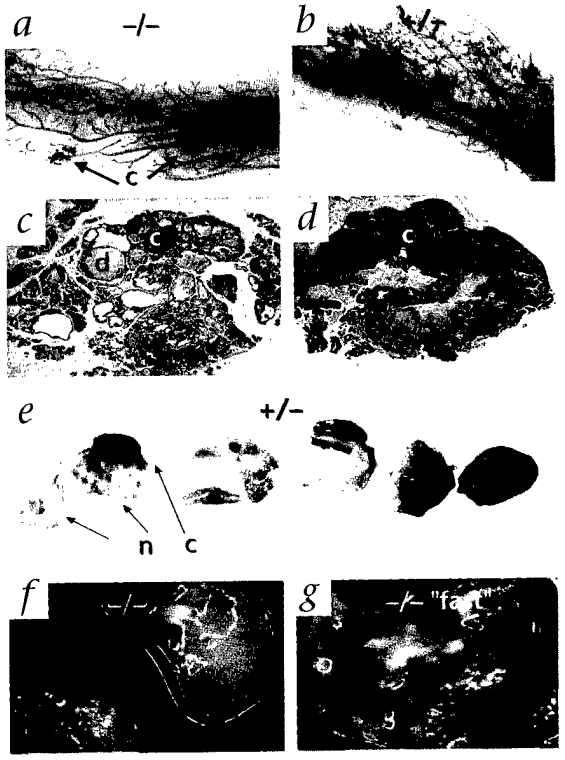

Fig. 5 Mammary fat pads and tumors. ***a–d***, Whole mounts of mammary fat pads without palpable tumor at 19 weeks (*a* and *b*) and histological sections of tumors at 26 weeks stained with hematoxylin and eosin (*c* and *d*) from *Mgat5*$^{-/-}$ (left column) and *Mgat5*$^{+/-}$ (right column) mice. ***e***, *LacZ* activity in mammary fat pads with low to high (left to right) tumor burden in PyMT *Mgat5*$^{+/-}$ mice. ***f*** and ***g***, PyMT *Mgat5*$^{-/-}$ tumors, one with low *LacZ* activity (*f*) and a fast-growing PyMT *Mgat5*$^{-/-}$ tumor (*g*). d, dysplasia and hyperplasia; c, carcinoma; n, mammary fat pad.

edges, with fine radial actin fibers extending into the cells (Fig. 6*a* and *b*). PyMT activates c-Src kinase, which phosphorylates paxillin, allowing its recruitment into focal adhesions found at the ruffling edges in PyMT *Mgat5*$^{+/-}$ tumor cells. Paxillin in focal adhesion complexes is a docking protein for other signaling proteins, including FAK, Csk, c-Src and PI3 kinase[31]. Membrane ruffling and filapodia formation requires PI3 kinase activation[32], which is also a direct target of PyMT oncogenesis. Indeed, inhibition of PI3 kinase with wortmannin decreased membrane ruffling in PyMT *Mgat5*$^{+/-}$ cells and increased actin stress fibers, creating a morphology similar to that of PyMT *Mgat5*$^{-/-}$ cells (Fig. 6*c*). To measure actin filament turnover, we treated cells with latrunculin-A, a compound that binds actin monomers and renders them incompetent for filament formation[33]. The loss of rhodamine–phalloidin-staining filaments was more rapid in PyMT *Mgat5*$^{+/-}$ than in PyMT *Mgat5*$^{-/-}$ tumor cells, indicating a slower turnover of focal adhesions in cells with the latter genotype (Fig. 6*g*).

D3-phosphoinosotides produced by PI3 kinase stimulate phosphorylation and activation of PKB. The amounts of PKB protein and phosphorylated PKB were decreased in PyMT *Mgat5*$^{-/-}$ tumors, whereas amounts of phosphorylated mitogen-activated protein (MAP) kinase were not different (Fig. 6*h*). The amounts of phosphorylated PKB as well as membrane ruffling were restored in PyMT *Mgat5*$^{-/-}$ tumors with the fast-growth phenotype (Fig. 6*h*, far right lane). However, the tumor cell population was heterogenous for the membrane ruffling phenotype (Fig. 6*d*).

The *Mgat5*-null mutation also affected focal adhesions in the absence of an oncogene. *Mgat5*$^{+/-}$ fibroblasts spread extensively and pseudopodia showed fine actin microfilament, whereas there were cortical stress fibers characteristic of non-motile cells in *Mgat5*$^{-/-}$ cells (Fig. 6*e* and *f*). The amount of phosphorylated PKB was also decreased, but amounts of phosphorylated MAP kinase were similar in fibroblasts expressing Mgat5 (Fig. 6*h*). The addition of serum induced rapid phosphorylation of MAP kinase and PKB, indicating that signaling potential was similar in mutant and wild-type cells. Therefore, the intrinsic defect in *Mgat5*$^{-/-}$ cells seems to be an inability to accelerate focal adhesion turnover and signaling through PI3 kinase/PKB as required for full transformation by PyMT.

Discussion

Here, we have shown that Mgat5 products are not required for embryonic development, but when expressed in cancer cells, they contribute directly to tumor growth and metastasis. Using the PyMT transgenic model of breast cancer, we examined early events in tumor formation as well as metastasis and secondary events associated with tumor progression. The initial appearance of tumors was delayed in PyMT *Mgat5*$^{-/-}$ mice compared with that in either *Mgat5*$^{+/-}$ or *Mgat5*$^{+/+}$ PyMT-trangenic mice. Tumor initiation occurred efficiently, as indicated by multi-focal tumor formation and involvement of 10 of 10 mammary fat pads in PyMT-transgenic mice of all *Mgat5* genotypes. The fraction of apoptotic tumor cells was small and similar in all genotypes. However, the proportion of proliferating cells in hyperplasia, dysplasia and carcinoma was less in PyMT *Mgat5*$^{-/-}$ mice than in similar tissues in mice expressing Mgat5. Tumor diameters and weights at the end of the experiment showed decrease of about 500% in tumor burden in the PyMT *Mgat5*$^{-/-}$ mice compared with that in the mice expressing Mgat5. Similar delays in tumor appearance have been seen in PyMT-transgenic mice on a *Grb2*$^{+/-}$ genetic background (an adapter protein in the Ras pathway[34]) and also on an *Ets-2*$^{+/-}$ background (a transcription factor downstream of Ras; ref. 35). However, the decrease in tumor growth rates was more substantial here. The incidence of lung metastases was also considerably decreased, approximately 5% in Mgat5-deficient mice. Suppression of tumor growth and metastasis has been reported for somatic tumor cell mutants lacking Mgat5 transplanted into syngenic mice[10]. This indicates that decreased tumor growth in PyMT *Mgat5*$^{-/-}$ mice is likely a tumor-cell-autonomous phenotype rather than being host-mediated, and prompted further examination of the PyMT tumor cells.

The amounts of phosphorylated PKB were decreased in PyMT *Mgat5*$^{-/-}$ tumor cells, whereas phosphorylated MAP kinase amounts were unaffected, indicating that PyMT-dependent PI3 kinase and PKB activation is blocked by the *Mgat5*$^{-/-}$ mutation. The PyMT protein is tyrosine-phosphorylated at Y315/Y322, creating binding sites for p85, the regulatory subunit of PI3 kinase[25]. The Asn-Pro-Thr-Tyr motif at position 250 is also phosphorylated, creating a binding site for the phosphotyrosine-binding domain of Src homology 2 domain-containing (Shc) protein[29]. Mutations in either domain of PyMT compromise its transforming activity[27], creating a growth delay similar to that in PyMT *Mgat5*$^{-/-}$ mice. Integrin-mediated cell motility and invasion by mammary epithelial cells in culture depend on activation of PI3 kinase, which acts downstream of Rac and Cdc42 GTPases[36]. PI3 kinase increases the amounts of D-3 phosphoinositide, which is

required for PKB activation, actin microfilament re-organization, membrane ruffling, and cell motility[32,37]. Here, PyMT *Mgat5*$^{-/-}$ tumor cells on fibronectin-coated plastic were deficient in membrane ruffling, actin was organized as stress fibers and turnover was slower. The α and β chains of integrin receptors each have multiple N-glycosylation sites, and MGAT5 products are present at a fraction of the glycosylation sites on $\alpha_5\beta_1$ fibronectin receptor[17,18]. Overexpression of MGAT5 in epithelial cells enhanced cell motility and increased MGAT5 products on $\alpha_1\beta_5$, indicating that enzyme activity is not saturating in epithelial cells before transformation[14]. Therefore, integrins may be essential target glycoproteins modified by MGAT5 products to effect the increase in focal adhesion turnover, cell migration and tumor growth.

Our results show that in the absence of Mgat5 products, PyMT-induced activation of PI3 kinase and PKB is not sufficient for optimal tumor growth and metastasis. Furthermore, additional genetic or epigenetic event(s) in the tumor cells enabled 5 of 140 PyMT *Mgat5*$^{-/-}$ tumors to overcome growth suppression. This was accompanied by increased PKB activation and active membrane ruffling. Similarly, secondary events restoring tumor growth have been found in mice with a mutant PyMT transgene deficient in P85/PI3 kinase binding. Tumors in these mice express more c-ErbB2 and c-ErbB3 receptors, which may compensate for the loss of PyMT activity[27]. These results indicate that the dependence on MGAT5 products for tumor growth may be diminished with secondary mutations that amplify oncogene signals downstream of focal-adhesions, and might include increased activity of gene products such as c-Src, PI3 kinase, PKB or loss of phosphatase and tensin homolog.

LacZ expression from the *Mgat5* targeted locus was greater in tumors than in normal mammary fat pads, indicating that the PyMT oncogene is a positive regulator of the *Mgat5* promoter. Furthermore, LacZ expression was increased in the fast-growing *Mgat5*$^{-/-}$ tumors that overcame growth suppression. *LacZ* expression was considerably higher in PyMT *Mgat5*$^{+/-}$ tumors than in PyMT *Mgat5*$^{-/-}$ tumors, indicating that Mgat5 products also positively regulate *Mgat5* transcription.

The precise location of the MGAT5 products on specific glycoprotein(s) and their role in regulating tumor growth and metastasis remains to be determined. However, MGAT5 products on adhesion receptors may create steric hindrance that destabilizes agonist-dependent clusters in the plane of the membrane. Adhesion receptors are highly engaged and turnover is slow in quiescent substratum-attached cells. Cell motility requires a decrease in the proportion of stable receptor complexes to allow greater focal adhesion turnover. PyMT oncogenesis induces *Mgat5* gene expression and increases Mgat5 glycan products, which in turn stimulate focal adhesion turnover and tumor cell growth. Thus, Mgat5 glycan products seem to be potent downstream effectors of PyMT dependent oncogenesis. The role of MAGT5 products in normal physiological process is less apparent, but our observations of the *Mgat5*$^{-/-}$ mouse indicate they may regulate cell interactions affecting leukocyte migration, cell interactions with basement membranes in kidney glomeruli, and T-cell-receptor responses to antigens.

Our findings indicate that inhibitors of MGAT5 may be useful in the treatment of cancer by targeting their dependency on focal adhesion signaling for proliferation. Indeed, swainsonine, a competitive inhibitor of Golgi β-mannosidase II, has anti-cancer activity in mice[38,39]. This compound partially blocks Mgat5 products by diverting the biosynthesis pathway upstream of Mgat5 enzyme. In a phase I clinical trial of cancer patients, swainsonine treatment produced responses with mild side effects[40]. However, an MGAT5 inhibitor may provide a more-complete and specific block of the MGAT5 products. Our study

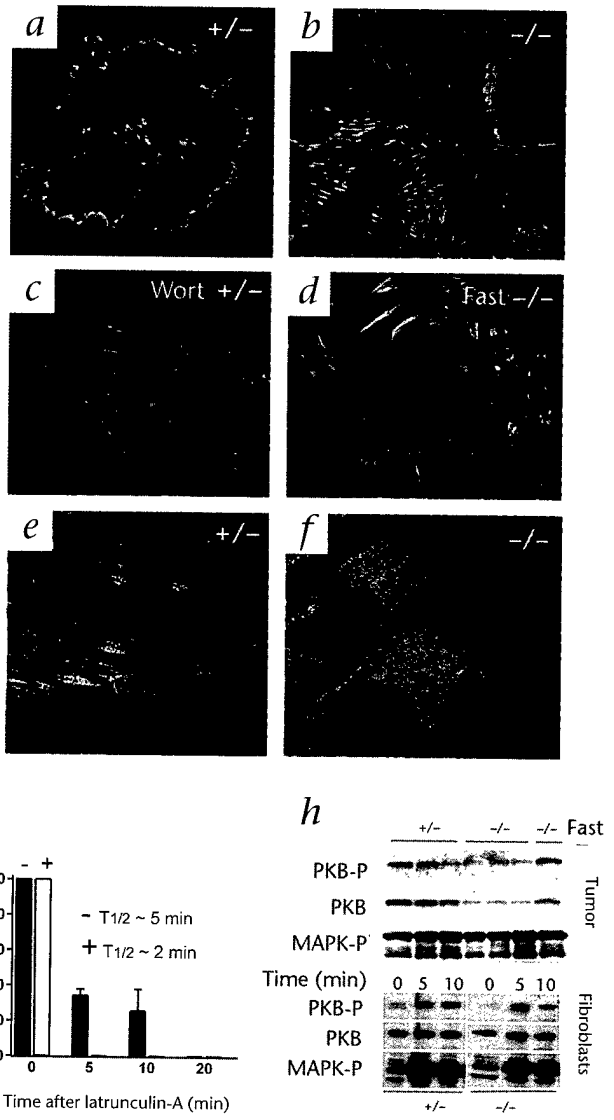

Fig. 6 Suppression of membrane ruffling, actin filament turnover and PKB phosphoprotein in PyMT *Mgat5*$^{-/-}$ tumor cells. ***a–f***, Cells were plated on glass cover slips coated with fibronectin, fixed and stained with the nuclear stain Hoechst322, actin-specific rhodamine–phalloidin and FITC-conjugated antibody against paxillin. *a* and *b*, Paxillin (green) is present at the ends of microfilaments (red) in focal adhesions of *Mgat5*$^{+/-}$ (*a*) but not *Mgat5*$^{-/-}$ (*b*) fibroblasts. *c*, PyMT *Mgat5*$^{+/-}$ tumors on fibronectin treated with 100 nM wortmannin for 18 h. *d*, PyMT *Mgat5*$^{-/-}$ tumor cell from a fast-growing tumor (representative of 5 of 140 tumors) that escaped *Mgat5*$^{-/-}$ growth suppression. *e* and *f*, Embryonic fibroblasts. *Mgat5*$^{+/-}$ cells spread more extensively, therefore the nucleus in *e* is out of view to the left. ***g***, Actin microfilament decay in the presence of 0.5 μM latrunculin-A, determined by the fraction of cells staining with rhodamine–phalloidin. ***h***, Mouse tumors were homogenized and detergent extracts were separated by SDS–PAGE and assessed by western blot analysis with antibodies against phosphorylated MAP kinase (Thr202/Tyr204) and PKB and phosphorylated PKB. Fast, fast-growing tumor. Below, The procedure was repeated with primary embryonic fibroblasts growth-arrested in serum-free medium and re-stimulated with serum for 5 and 10 min.

shows that suppression of Mgat5 activity is not toxic, and sheds light on the molecular mechanism of tumor growth suppression, as well as the possibilities of acquired resistance to Mgat5 inhibition in tumors.

Methods

Mutation of the *Mgat5* gene. A genomic library from strain 129/sv mice was screened with a *Mgat5* cDNA probe. A 13.5-kb genomic clone containing the 205-nucleotide 5′ untranslated region and 241 nucleotides spanning the first coding exon was used to construct the *Mgat5* targeting vector. The *Mgat5* targeting vector was constructed with *lacZ* replacing the coding region of the first exon. The targeting vector was linearized by digestion with *Not*I and electroporated into R1 ES cells, and transfected cells were selected in the presence of G418 and gancyclovir as described[41]. DNA from drug-resistant colonies was digested with *Pst*I and screened for homologous recombination by Southern blot analysis using a 1.7-kb *Pst*I–*Xba*I genomic fragment external to the targeting vector. Two *Mgat5*$^{+/-}$ ES cell lines were aggregated with blastocysts from CD-1 mice and implanted into pseudo-pregnant CD-1 females. The resultant chimeras were mated with 129/sv females. Heterozygous progeny were intercrossed to generate *Mgat5*$^{-/-}$ mice, and experiments were done on the 129/sv background. For histology, mice were perfused with 10% phosphate-buffered formalin *in vivo* and tissues were embedded in paraffin, sectioned, and stained with hematoxylin and eosin. To detect β-galactosidase (*lacZ*) activity, tissues were fixed in 0.2% glutaraldehyde for 30 min, washed in phosphate-buffered saline, and incubated overnight in X-gal staining solution (1 mg/ml 4-chloro-5-bromo-3-indolyl-β-galactoside (X-gal), 4 mM $K_4Fe(CN)_6 \cdot 3H_2O$, 4 mM $K_3Fe(CN)_6$, 2 mM $MgCl_2$, 0.01% deoxycholate and 0.02% Nonidet P-40 in 0.1 M sodium phosphate, pH 7.3). After being stained, samples were further fixed in 10% phosphate-buffered formalin.

Tumor growth and metastasis in PyMT-transgenic mice. Transgenic mice expressed the PyMT oncogene under the control of the mouse mammary tumor virus long terminal repeat[28]. Male PyMT *Mgat5*$^{+/-}$ mice on a 129sv × FVB-129/sv background were crossed with 129sv *Mgat5*$^{+/-}$ female mice littermates lacking the PyMT gene. The progeny were genotyped by PCR, and examined by palpation for tumors on a weekly basis. Once tumors were detected, they were measured with callipers weekly. Mice were killed when their tumor burden reached about 50% of their body weight, and lungs were resected and surface metastatic foci were counted with a dissection microscope. Immunohistochemisty was done using a 1:1,000 dilution of biotinylated antibody against proliferating cell nuclear antigen (Novocastra, Newcastle, UK) and developed using strepavidin detection system (Signet, Dedham, Massachusetts). Apoptosis was assessed using DNA end-labeling and immunohistochemical detection.

L-PHA lectin, western blot analysis and Mgat5 assay. Tumors from the mice were homogenized in 10 volumes of RIPA buffer; 50 mM Tris-HCl, pH7.5, 150 mM NaCl, 1% Triton-X100, 1% deoxycholate, 0.1% SDS, 100 μM orthovanadate, 1 mM PMSF and protease inhibitor 'cocktail' (Boehringer). Cell lysates were prepared in the same buffer. Detergent extracts were clarified by centrifugation, and proteins were separated by SDS–PAGE, transferred electrophoretically to PVDF membrane and assessed by western blot analysis using 1:500 dilutions of antibodies against phosphorylated MAP kinase (Thr202/Tyr204), PKB and phosphorylated PKB (NEB). For lectin blots, membranes were probed with 0.5 μg/ml L-PHA, followed by incubation with a rabbit antibody against L-PHA (1:1,000 dilution) and with HRP-conjugated donkey antibody against rabbit (Amersham). Mgat5 enzyme activity in tissue homogenates was determined as transfer of ^{3}H-GlcNAc from UDP-6-^{3}H-GlcNAc (Amersham) to the synthetic acceptor GlcNAcβ1-2Manβ1-6Glcβ1-octyl per mg of lysate protein, as described[14].

Focal adhesion and actin microfilament turnover. PyMT mammary tumor cells and fibroblasts from embryos at embryonic day 13.5 were extracted from tissues samples with trypsin and cultured for 2 weeks in alpha-modified Eagle medium plus 10% FCS. Cells were plated overnight on glass slides coated with 1 μg/ml fibronectin in serum-free alpha-modified Eagle medium. The cells were then fixed in 3.7% paraformaldehyde, washed with 0.2% Nonidet P-40 in phosphate-buffered saline and stained with rhodamine–phalloidin, 1:50 dilution of antibodies against paxillin (Transduction Laboratories, Lexington, Kentucky), and Hoechst 33258 stain according to the manufacturer's instructions. Fluorescence images of the cells were obtained using a deconvolution microscope and digital capture of data. Latrunculin-A, an actin monomer-binding drug that renders the monomers incompetent for filament formation, was added to cells at a concentration of 0.5 μM, and the percentage of cells with actin microfilaments was determined by staining with rhodamine–phalloidin.

Acknowledgments

The authors thank C. Warren, S. Kulkarni and P. Cheung for suggestions. This research was supported by grants from National Cancer Institute of Canada, the Mizutani Foundation, the National Science and Engineering Research Council of Canada, and GlycoDesign (Toronto, Canada). W.J.M. is supported by a Medical Research Council Scientist Award.

RECEIVED 20 SEPTEMBER; ACCEPTED 29 DECEMBER 1999

1. Yamashita, K., Ohkura, T., Tachibana, Y., Takasaki, S. & Kobata, A. Comparative study of the oligosaccharides released from baby hamster kidney cells and their polyoma transformant by hydrazinolysis. *J. Biol .Chem.* **259**, 10834–10840 (1984).
2. Pierce, M. & Arango, J. Rous sarcoma virus-transformed baby hamster kidney cells express higher levels of asparagine-linked tri- and tetraantennary glycopeptides containing [GlcNAc-β(1,6)Man-α(1,6)Man] and poly-N-acetyllactosamine sequences than baby hamster kidney cells. *J. Biol. Chem.* **261**, 10772–10777 (1986).
3. Cummings, R.D., Trowbridge, I.S. & Kornfeld, S. A mouse lymphoma cell line resistant to the leukoagglutinating lectin from *Phaseolus vulgaris* is deficient in UDP-GlcNAc:α-D-mannoside β1,6 N-acetylglucosaminyltransferase. *J. Biol. Chem.* **257**, 13421–13427 (1982).
4. Shoreibah, M. *et al.* Isolation, characterization, and expression of cDNA encoding *N*-Acetylglucosaminyltransferase V. *J. Biol. Chem.* **268**, 15381–15385 (1993).
5. Cummings, R.D. & Kornfeld, S. Characterization of the structural determinants required for the high affinity interaction of asparagine-linked oligosaccharides with immobilized *Phaseolus vulgaris* leukoagglutinating and erythroagglutinating lectin. *J. Biol. Chem.* **257**, 11230–11234 (1982).
6. Fernandes, B., Sagman, U., Auger, M., Demetriou, M. & Dennis, J.W. β1-6 branched oligosaccharides as a marker of tumor progression in human breast and colon neoplasia. *Cancer Res.* **51**, 718–723 (1991).
7. Seelentag, W.K., *et al.* Prognostic value of β1,6-branched oligosaccharides in human colorectal carcinoma. *Cancer Res.* **58**, 5559–5564 (1998).
8. Yamashita, K., Tachibana, Y., Ohkura, T. & Kobata, A. Enzymatic basis for the structural changes of asparagine-linked sugar chains of membrane glycoproteins of baby hamster kidney cells induced by polyoma transformation. *J. Biol. Chem.* **260**, 3963–3969 (1985).
9. Dennis, J.W., Kosh, K., Bryce, D.-M. & Breitman, M.L. Oncogenes conferring metastatic potential induce increased branching of Asn-linked oligosaccharides in rat2 fibroblasts. *Oncogene* **4**, 853–860 (1989).
10. Dennis, J.W., Laferte, S., Waghorne, C., Breitman, M.L. & Kerbel, R.S. β1-6 branching of Asn-linked oligosaccharides is directly associated with metastasis. *Science* **236**, 582–585 (1987).
11. Kang, R. *et al.* Transcriptional regulation of the N-acetylglucosaminyltranserase V gene in human bile duct carcinoma cells (HuCC-T1) is mediated by Ets-1. *J. Biol.Chem.* **271**, 26706–26712 (1996).
12. Chen, L., Zhang, W., Fregien, N. & Pierce, M. The her-2/neu oncogene stimulates the transcription of N-acetylglucosaminyltransferase V and expression of its cell surface oligosaccharide products. *Oncogene* **17**, 2087–2093 (1998).
13. Lu, Y., Pelling, J.C. & Chaney, W.G. Tumor cells surface β1-6 branched oligosaccharides and lung metastasis. *Clin. Exp. Metastasis* **12**, 47–54 (1994).
14. Demetriou, M., Nabi, I.R., Coppolino, M., Dedhar, S. & Dennis, J.W. Reduced contact inhibition and substratum adhesion in epithelial cells expressing GlcNAc-transferase V. *J. Cell Biol.* **130**, 383–392 (1995).
15. Seberger, P.J. & Chaney, W.G. Control of metastasis by asn-linked, β1-6 branched oligosaccharides in mouse mammary cancer cells. *Glycobiology* **9**, 235–241 (1999).
16. Do, K.-Y., Fregien, N., Pierce, M. & Cummings, R.D. Modification of glycoproteins by *N*-acetylglucosaminyltransferase V is greatly influenced by accessibility of the enzyme to oligosacharide acceptors. *J. Biol. Chem.* **269**, 23456–23464 (1994).
17. Nakagawa, H., *et al.* Detailed oligosaccharide structures of human integrin alpha 5 beta 1 analyzed by a three-dimensional mapping technique. *Eur. J. Biochem.* **237**, 76–85 (1996).
18. Asada, M., Furukawa, K., Kantor, C., Gahmberg, C.G. & Kobata, A. Structural study of the sugar chains of human leukocyte cell adhesion molecules CD11/CD18. *Biochemistry* **30**, 1561–1571 (1991).
19. Skelton, T.P., Zeng, C., Nocks, A. & Stamenkovic, I. Glycosylation provides both stimulatory and inhibitory effects on cell surface and soluble CD44 binding to hyaluronan. *J. Cell Biol.* **140**, 431–446 (1998).
20. Diamond, M.S., Staunton, D.E., Martin, S.D. & Springer, T.A. Binding of the integrin Mac-1 (CD11b/CD18) to the third immunoglobulin-like domain of ICAM-1 (CD54) and its regulation by glycosylation. *Cell* **65**, 961–971 (1991).
21. McEvoy, L.M., Sun, H., Frelinger, J.G. & Butcher, E.C. Anti-CD43 inhibition of T cell

homing. *J. Exp. Med.* **185**, 1493–1498 (1997).
22. Verbeek, B.S. *et al.* c-Src protein expression is increased in human breast cancer. An immunohistochemical and biochemical analysis. *J. Pathol.* **180**, 383–388 (1996)
23. Liu, A.X., *et al.* AKT2, a member of the protein kinase B family, is activated by growth factors, v-Ha-ras, and v-src through phosphatidylinositol 3-kinase in human ovarian epithelial cancer cells. *Cancer Res.* **58**, 2973–2977 (1998).
24. Dilworth, S.M. *et al.* Transformation by polyoma virus middle T-antigen involves the binding and tyrosine phosphorylation of Shc. *Nature* **367**, 87–90 (1994).
25. Whitman, M., Kaplan, D.R., Schaffhausen, B., Cantley, L. & Roberts, T.M. Association of phosphatidylinositol kinase activity with polyoma middle-T competent for transformation. *Nature* **315**, 239–242 (1985).
26. Guy, C.T., Muthuswamy, S.K., Cardiff, R.D., Soriano, P. & Muller, W.J. Activation of the c-Src tyrosine kinase is required for the induction of mammary tumors in transgenic mice. *Genes Dev.* **1**, 23–32 (1994).
27. Webster, M.A. *et al*Requirement for both Shc and phosphatidylinositol 3′ kinase signaling pathways in polyomavirus middle T-mediated mammary tumorigenesis. *Mol. Cell. Biol.* **18**, 2344–2359 (1998).
28. Guy, C.T., Cardiff, R.D. & Muller, W.J. Induction of mammary tumors by expression of polyomavirus middle T oncogene: a transgenic mouse model for metastatic disease. *Mol. Cell. Biol.* **12**, 954–961 (1992).
29. Bronson, R., Dawe, C., Carroll, J. & Benjamin, T. Tumor induction by a transformation-defective polyoma virus mutant blocked in signaling through Shc. *Proc. Natl. Acad. Sci. USA* **94**, 7954–7958 (1997).
30. Granovsky, M. *et al.* GlcNAc-transferase V and core 2 GlcNAc-transferase expression in the developing mouse embryo. *Glycobiology* **5**, 797–806 (1995).
31. Turner, C.E. Molecules in focus, paxillin. *Int. J. Biol. Macromol.* **30**, 955–959 (1998).
32. Reif, K., Nobes, C.D., Thomas, G., Hall, A. & Cantrell, D.A. phosphatidylinositol 3-kinase signals activate a selective subset of Rac/Rho dependent effector pathways. *Curr. Biol.* **6**, 1445–1455 (1996).
33. Spector, I., Shochet, N.R., Blasberger, D. & Kashman, Y. Latrunculins, novel marine macrolides that disrupt microfilament organization and affect cell growth: I. Comparison with cytochalasin D. *Cell Motil. Cytoskeleton* **13**, 127–124 (1989).
34. Cheng, A.M. *et al.* Mammalian Grb2 regulates multiple steps in embryonic development and malignant transformation. *Cell* **95**, 793–803 (1999).
35. Neznanov, N. *et al.* A single targeted Ets2 allele restricts development of mammary tumors in transgenic mice. *Cancer Res.* **59**, 4242–4246 (1999).
36. Keely, P.J., Westwick, J.K., Whitehead.I.P., Der, C.J. & Parise, L.V. Cdc42 and Rac1 induce integrin-mediated cell motility and invasiveness through PI(3)K. *Nature* **390**, 632–636 (1997).
37. King, W.G., Mattaliano, M.D., ChanT.O., Tsichlis, P.N. & Brugge, J.S. Phosphatidylinositol 3-kinase is required for integrin-stimulated AKT and Raf-1/mitogen-activated protein kinase pathway activation. *Mol. Biol. Cell* **17**, 4406–4418 (1997).
38. Humphries, M.J., Matsumoto, K., White, S.L. & Olden, K. Oligosaccharide modification by swainsonine treatment inhibits pulmonary colonization by B16-F10 murine melanoma cells. *Proc. Natl. Acad. Sci. USA* **83**, 1752–1756 (1986).
39. Dennis, J.W. Effects of swainsonine and polyinosinic-polycytidylic acid on murine tumor cell growth and metastasis. *Cancer Res.* **46**, 5131–5136 (1986).
40. Goss, P.E., Baptiste, J., Fernandes, B., Baker, M. & Dennis, J.W. A study of swainsonine in patients with advanced malignancies. *Cancer Res.* **54**, 1450–1457 (1994).
41. Hasty, P. & Bradley, A. in *Gene Targeting. A Practical Approach* (ed. Joyner, A.) 138–180 (IRL Oxford Press, 1993).

Glucose and insulin tolerance tests

Glucose tolerance tests were performed in awake mice after a 12-h fast[5]. Insulin tolerance tests were performed in awake mice after a 6-h fast[5].

Whole-body, skeletal muscle and liver glucose flux *in vivo*

Hyperinsulinaemic–euglycaemic clamp studies with uptake of [^{14}C]2-deoxyglucose into individual tissues were performed as described[23] in awake female mice at 6 months of age. Insulin was infused continuously for 120 min at 2.5 mU per kg (body weight) per min. Basal and insulin-stimulated rates of glucose turnover were measured with continuous [3-^{3}H]glucose infusion.

Phosphoinositide-3-OH kinase activity

Mice were fasted for 16–18 h, injected i.v. with saline or insulin (10 U per kg (body weight)) and killed 3 min after injection. Tissues were collected and frozen. PI(3)K activity was measured in phosphotyrosine immunoprecipitates (monoclonal antibody PY99, Santa Cruz Biotechnology, Santa Cruz, CA) from muscle and liver lysates as described[24].

Tissue triglyceride content

Triglyceride content in quadriceps muscle and liver was determined as described[25].

Adipocyte TNF-α mRNA and serum TNF-α levels

RNA was extracted from WAT and BAT using Trizol (GibcoBRL) and the expression of TNF-α mRNA relative to GAPDH mRNA or 18S ribosomal RNA was determined by real-time PCR (TaqMan, PE Systems). Serum TNF-α levels were determined in serum samples (50 μl) using the mouse TNF-α ELISA (Endogen). Both mRNA and serum levels were assessed in age- and sex-matched male and female mice at 12–13 and 26 weeks of age.

Statistical analysis

Data are expressed as mean ± s.e.m. Differences between two groups were assessed using the unpaired two-tailed *t*-test and among more than two groups by analysis of variance (ANOVA). Data involving more than two repeated measures (glucose and insulin tolerance tests) were assessed by repeated measures ANOVA. Analyses were performed using Statview Software (BrainPower, Calabasas, CA).

Received 29 August; accepted 14 November 2000.

1. Cline, G. W. *et al.* Impaired glucose transport as a cause of decreased insulin-stimulated muscle glycogen synthesis in type 2 diabetes. *N. Engl. J. Med.* **341,** 240–246 (1999).
2. Roden, M. & Shulman, G. I. Applications of NMR spectroscopy to study muscle glycogen metabolism in man. *Annu. Rev. Med.* **50,** 277–290 (1999).
3. Defronzo, R. A. Pathogenesis of type 2 diabetes: metabolic and molecular implications for identifying diabetes genes. *Diabetes Rev.* **5,** 177–269 (1997).
4. Shepherd, P. R. & Kahn, B. B. Glucose transporters and insulin action–implications for insulin resistance and diabetes mellitus. *N. Engl. J. Med.* **341,** 248–257 (1999).
5. Abel, E. D. *et al.* Cardiac hypertrophy with preserved contractile function after selective deletion of GLUT4 from the heart. *J. Clin. Invest.* **104,** 1703–1714 (1999).
6. Zisman, A. *et al.* Targeted disruption of the glucose transporter 4 selectively in muscle causes insulin resistance and glucose intolerance. *Nature Med.* **6,** 924–928 (2000).
7. Ross, S. R. *et al.* A fat-specific enhancer is the primary determinant of gene expression for adipocyte P2 *in vivo*. *Proc. Natl Acad. Sci. USA* **87,** 9590–9504 (1990).
8. Zambrowicz, B. P. *et al.* Disruption of overlapping transcripts in the ROSA β geo 26 gene trap strain leads to widespread expression of β-galactosidase in mouse embryos and hematopoietic cells. *Proc. Natl Acad. Sci. USA* **94,** 3789–3794 (1997).
9. Soriano, P. Generalized lacZ expression with the ROSA26 Cre reporter strain. *Nature Genet.* **21,** 70–71 (1999).
10. Katz, E. B., Stenbit, A. E., Hatton, K., Depinho, R. & Charron, M. J. Cardiac and adipose tissue abnormalities but not diabetes in mice deficient in GLUT4. *Nature* **377,** 151–155 (1995).
11. Donoghue, M. J., Alvarez, J. D., Merlie, J. P. & Sanes, J. R. Fiber type- and position-dependent expression of a myosin light chain- CAT transgene detected with a novel histochemical stain for CAT. *J. Cell Biol.* **115,** 423–434 (1991).
12. West, D. B., Boozer, C. N., Moody, D. L. & Atkinson, R. L. Dietary obesity in nine inbred mouse strains. *Am. J. Physiol.* **262,** R1025–R1032 (1992).
13. Boden, G. Role of fatty acids in the pathogenesis of insulin resistance and NIDDM. *Diabetes* **46,** 3–10 (1997).
14. Muoio, D. M. *et al.* Leptin directly alters lipid partitioning in skeletal muscle. *Diabetes* **46,** 1360–1363 (1997).
15. Burcelin, R. *et al.* Acute intravenous leptin infusion increases glucose turnover but not skeletal muscle glucose uptake in ob/ob mice. *Diabetes* **48,** 1264–1269 (1999).
16. Hotamisligil, G. S. & Spiegelman, B. M. Tumor necrosis factor alpha: a key component of the obesity-diabetes link. *Diabetes* **43,** 1271–1278 (1994).
17. Griffin, M. E. *et al.* Free fatty acid-induced insulin resistance is associated with activation of protein kinase C theta and alterations in the insulin signaling cascade. *Diabetes* **48,** 1270–1274 (1999).
18. Dresner, A. *et al.* Effects of free fatty acids on glucose transport and IRS-1-associated phosphatidylinositol 3-kinase activity. *J. Clin. Invest.* **103,** 253–9 (1999).
19. Mueller, W. M. *et al.* Evidence that glucose metabolism regulates leptin secretion from cultured rat adipocytes. *Endocrinology* **139,** 551–558 (1998).
20. Sivitz, W. I., Walsh, S. A., Morgan, D. A., Thomas, M. J. & Haynes, W. G. Effects of leptin on insulin sensitivity in normal rats. *Endocrinology* **138,** 3395–3401 (1997).
21. Tozzo, E., Gnudi, L. & Kahn, B. B. Amelioration of insulin resistance in streptozotocin diabetic mice by transgenic overexpression of GLUT4 driven by an adipose-specific promoter. *Endocrinology* **138,** 1604–1611 (1997).
22. Cushman, S. W. & Salans, L. B. Determinations of adipose cell size and number in suspensions of isolated rat and human adipose cells. *J. Lipid Res.* **19,** 269–273 (1978).
23. Kim, J. K., Gavrilova, O., Chen, Y., Reitman, M. L. & Shulman, G. I. Mechanism of insulin resistance in A-ZIP/F-1 fatless mice. *J. Biol. Chem.* **275,** 8456–8460 (2000).
24. Kim, Y. B. *et al.* Glucosamine infusion in rats rapidly impairs insulin stimulation of phosphoinositide 3-kinase but does not alter activation of Akt/protein kinase B in skeletal muscle. *Diabetes* **48,** 310–320 (1999).
25. Storlien, L. H. *et al.* Influence of dietary fat composition on development of insulin resistance in rats. Relationship to muscle triglyceride and omega-3 fatty acids in muscle phospholipid. *Diabetes* **40,** 280–289 (1991).

Acknowledgements

This work was supported by NIH Grants (to E.D.A., G.I.S. and B.B.K.) and an American Diabetes Association award to B.B.K. E.D.A. was the recipient of awards from the Robert Wood Johnson Foundation and the Eleanor and Miles Shore Scholars in Medicine Fellowship (Harvard Medical School). O.P. was supported by grants from the ALFEDIAM Society and Nestlé, France; and O.B. by the Human Frontier Sciences Program. We thank H. Chen for performing the TaqMan assays; P. She and M.A. Magnusen for breeding *aP2–Cre* mice with *Rosa26–lacZ* floxed mice; G. Hotamisligil for helpful advice; and C. Oberste-Berghaus and M. Pham for expert assistance.

Correspondence and requests for materials should be addressed to B.B.K. (e-mail: bkahn@caregroup.harvard.edu).

Negative regulation of T-cell activation and autoimmunity by *Mgat5 N*-glycosylation

Michael Demetriou*†‡, Maria Granovsky*‡, Sue Quaggin* & James W. Dennis*§

** Samuel Lunenfeld Research Institute, Mount Sinai Hospital, 600 University Avenue, R988, Toronto, Ontario M5G 1X5, Canada*
† Division of Neurology, Department of Medicine, University of Toronto
§ Department of Molecular & Medical Genetics, University of Toronto
‡ These authors contributed equally to this work

T-cell activation requires clustering of a threshold number of T-cell receptors (TCRs) at the site of antigen presentation, a number that is reduced by CD28 co-receptor recruitment of signalling proteins to TCRs[1–5]. Here we demonstrate that a deficiency in β1,6 *N*-acetylglucosaminyltransferase V (Mgat5), an enzyme in the *N*-glycosylation pathway, lowers T-cell activation thresholds by directly enhancing TCR clustering. Mgat5-deficient mice showed kidney autoimmune disease, enhanced delayed-type hypersensitivity, and increased susceptibility to experimental autoimmune encephalomyelitis. Recruitment of TCRs to agonist-coated beads, TCR signalling, actin microfilament re-organization, and agonist-induced proliferation were all enhanced in *Mgat5*$^{-/-}$ T cells. *Mgat5* initiates GlcNAc β1,6 branching on *N*-glycans, thereby increasing *N*-acetyllactosamine[6], the ligand for galectins[7,8], which are proteins known to modulate T-cell proliferation and apoptosis[9,10]. Indeed, galectin-3 was associated with the TCR complex at the cell surface, an interaction dependent on Mgat5. Pre-treatment of wild-type T cells with lactose to compete for galectin binding produced a phenocopy of *Mgat5*$^{-/-}$ TCR clustering. These data indicate that a galectin–glycoprotein lattice strengthened by Mgat5-modified glycans restricts TCR recruitment to the site of antigen presentation. Dysregulation of Mgat5 in humans may increase susceptibility to autoimmune diseases, such as multiple sclerosis.

Specific glycan structures regulate lymphocyte adhesion, recirculation and maturation, as demonstrated by the GDP-fucose deficiency in LADII patients[11], and immune defects associated with C2 *N*-acetylglucosamine (GlcNAc)-T(L)[12] or ST3Gal-I (ref. 13)

mutant mice. Depletion of the Mgat5-modified glycans by swainsonine, an inhibitor of α-mannosidase II, potentiates antigen-dependent T-cell proliferation[14]. Mgat5 catalyses the addition of β1,6-GlcNAc to *N*-glycan intermediates found on newly synthesized glycoproteins that transit the medial Golgi[15] (Fig. 1a). The glycans are elongated in *trans*-Golgi to produce tri (2,2,6) and tetra (2,4,2,6) antennary *N*-glycans, which are extended with *N*-acetyllactosamine (Gal-β1,4-GlcNAc) and polymeric forms of *N*-acetyllactosamine[6]. To further explore the function of Mgat5 in T-cell immunity, we examined Mgat5-deficient mice for evidence of immune dysfunction. *Mgat5*$^{-/-}$ mice are born healthy, and lack Mgat5 *N*-glycan products in all tissues examined[16]. At 3 months of age, peripheral white blood cells, erythrocyte and serum levels of immunoglobulin (Ig)M and IgG were comparable in Mgat5$^{-/-}$, *Mgat5*$^{+/-}$ and *Mgat5*$^{+/+}$ mice (data not shown). The CD4 and CD8 reactive T-cell populations in the spleen and thymus were also in the normal range (Fig. 1b, c). At 12–20 months of age, an increased incidence of leukocyte colonies in kidney and enlarged spleens was observed in *Mgat5*$^{-/-}$ mice. Furthermore, 32% of the *Mgat5*$^{-/-}$ (6 out of 19 mice) had macroscopic haematuria, mononuclear infiltrates and extensive accumulation of fibrin within Bowman's space, characteristic of proliferative glomerulonephritis (Fig. 1d). This form of renal injury is often observed in autoimmune-mediated glomerulonephritis. Milder renal defects were observed in 68% of the *Mgat5*$^{-/-}$ mice but not in the *Mgat5*$^{+/-}$ or Mgat5$^{+/+}$ mice.

To examine T-cell responses in the mice, we induced a type IV delayed-type hypersensitivity (DTH) reaction, and measured tissue swelling. The protein-reactive hapten oxazolone was applied topically to the backs of the mice, then again 4 d later to the right ear. Ear swelling in *Mgat5*$^{+/+}$ mice peaked 24 h after application, and swelling was completely gone by day 5. Ear swelling in *Mgat5*$^{-/-}$ mice attained a higher maximum between 48 and 72 h, and persisted for a longer time (Fig. 1e). To study T-cell-dependent autoimmunity *in vivo*[17], we induced experimental autoimmune encephalomyelitis (EAE) by immunizing mice with myelin basic protein (MBP) at three doses (25, 100 and 500 μg per mouse). At the lowest dose of MBP, the incidence of EAE was significantly greater in *Mgat5*-deficient mice. Furthermore, 25 and 100 μg doses of MBP produced more severe EAE in *Mgat5*$^{-/-}$ mice compared with wild-type littermates, characterized by an earlier onset, greater motor weakness and more days with disease (Table 1). Myelin injections of 500 μg induced disease in all mice with greater peak scores and no significant differences in disease incidence or severity between genotypes. These results indicate that mice lacking Mgat5-modified glycans are more susceptible to DTH and EAE autoimmune disease.

In vitro, splenic T cells from *Magt5*$^{-/-}$ mice hyperproliferated in response to anti-TCRα/β antibody (Fig. 2a). To examine this hypersensitivity in more detail, purified *ex vivo* T cells were cultured at low density and stimulated with increasing concentrations of soluble anti-CD3ε antibody in the presence or absence of anti-CD28

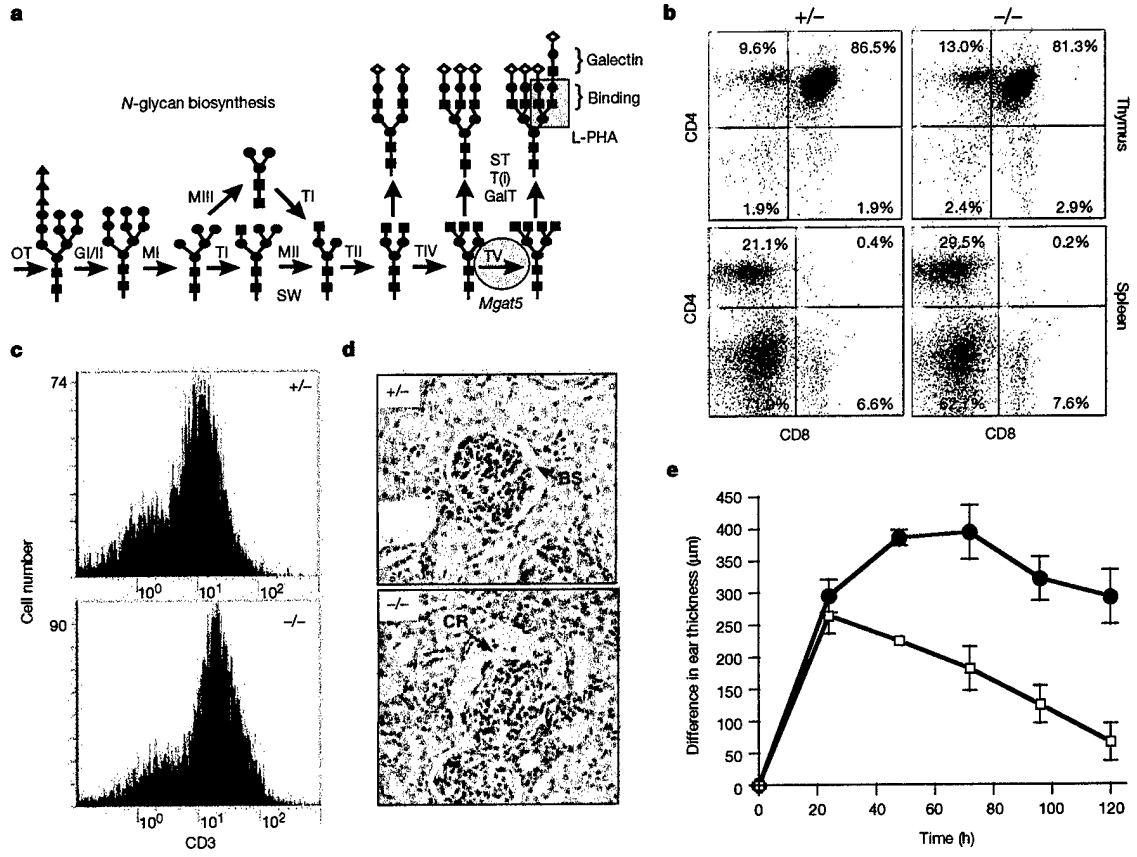

Figure 1 Immune phenotype in *Mgat5*$^{-/-}$ mice. **a**, The Golgi *N*-glycan biosynthesis pathway shows Mgat5 (TV) in the production of a tetra (2,4,2,6) antennary (numbers refer to the linkages of the antennae from left to right). OT, oligosaccharyltransferase; GI, GII, the α-glucosidases; TI, TII, TIV, TV, T(i), the β-*N*-acetylglycosaminyltransferases; MI, α1,3/6mannosidases MII, MIII, the α1,2mannosidases; Gal-T, β1,4-galactosyltransferases; ST, α-sialyltransferases; and SW, swainsonine block. The boxed structure Gal-β1,4-GlcNAc-β1,6(Gal-β1,4-GlcNAc-β1,2)Manα binds L-PHA. The galectin-binding disaccharide *N*-acetyllactosamine (Gal-β1,4-GlcNAc) is present in all antennae, and units are marked with red brackets in polylactosamine. **b**, Distribution of CD4$^+$ and CD8$^+$ cells in spleen and thymus by FACS analysis using FITC- or phycoerythrin-conjugated antibodies (Pharmingen) reactive to CD3ε, CD4 and CD8. **c**, TCR complex staining of spleen cells by FITC-anti-CD3ε antibodies and FACS analysis. **d**, Light microscopy of kidney showing cresentic glomerulonephritis with a large crescent (CR) of mononuclear cells and fibrin obliterating the Bowman's space (BS) in *Mgat5*$^{-/-}$ mice. **e**, DTH inflammatory response in *Mgat5*$^{-/-}$ (circles) and *Mgat5*$^{+/+}$ (squares) mice exposed to oxazolone (see Methods). The results are plotted as mean change ± standard error in ear thickness relative to the vehicle-treated left ear for seven *Mgat5*$^{-/-}$ and six *Mgat5*$^{+/+}$ control littermates. $P < 0.01$ with a student *t*-test comparing the genotypes at 2–5 d.

Table 1 Clinical observations of experimental autoimmune encephalomyelitis

Groups (dose)	Incidence of EAE	Peak score	Onset (days)	Days with disease	Deaths
Mgat5$^{+/+}$ (25 μg)	3/11	0.45 ± 0.24	24.0 ± 3.9	7.0 ± 3.9	0
Mgat5$^{-/-}$ (25 μg)	9/11*	1.82 ± 0.39†	19.8 ± 3.3†	11.5 ± 3.0†	1
Mgat5$^{+/+}$ (100 μg)	10/10	1.6 ± 0.22	25.0 ± 2.2	18.5 ± 2.2	0
Mgat5$^{-/-}$ (100 μg)	10/10	2.1 ± 0.34†	17.6 ± 2.9†	23.3 ± 3.5†	1
Mgat5$^{+/+}$ (500 μg)	12/12	3.0 ± 0.43	8.9 ± 1.2	27.9 ± 4.0	3
Mgat5$^{-/-}$ (500 μg)	12/12	2.83 ± 0.38	9.3 ± 0.95	27.2 ± 2.9	2

Disease severity was scored on a scale of 0–5 with: 0, no illness; 1, limp tail; 2, limp tail and hindlimb weakness; 3, hindlimb paralysis; 4, forelimb weakness/paralysis and hindlimb paralysis; and 5, moribundity or death. Means ± standard error of incidence, peak score and days with disease were calculated using the total number of mice injected per dose as the denominator. The mean ± standard error for day of onset was determined by only using those mice that developed diseases.
*Contingency test, $P < 0.001$.
† Mann–Whitney *U*-test comparing genotypes for significant differences at $P < 0.05$.

antibody (Fig. 2b). Both the Mgat5 deficiency and CD28 engagement reduced the requirements for TCR agonist as indicated by D_{50} values, and were additive when combined (Fig. 2c). Furthermore, the apparent Hill coefficient (n_H), a measure of synchrony in the responding cell population, was increased by both the Mgat5 deficiency and by CD28 engagement. Therefore, the stimulatory effects of the *Mgat5* mutation and CD28 co-receptor engagement were additive and similar in potency.

Alterations in cell-surface TCR complex levels and intracellular signalling potential of T cells were examined and discounted as possible causes of the *Mgat5*$^{-/-}$ hypersensitivity. The Mgat5 deficiency did not significantly alter cell-surface expression of CD3, CD4, CD8, TCRα/β, CD28 or CTLA-4 glycoproteins in resting T cells (Fig. 1b, c; and data not shown). Intracellular signalling potential in *Mgat5*$^{-/-}$ T cells is normal, as treatment with the phorbol ester 12-*O*-tetradecanoylphorbol-13-acetate (TPA) and the Ca^{2+} ionophore ionomycin stimulated T cells equally well from mice of both genotypes (Fig. 2d).

We next examined the relationship between cell-surface *Mgat5*-modified glycans and T-cell activation. Leukoagglutinin (L-PHA) is a tetravalent plant lectin and is a commonly used T cell mitogen that binds specifically to Mgat5-modified glycans. *Mgat5*$^{-/-}$ T cells were completely unresponsive to L-PHA, confirming that Mgat5-modified glycans are required for stimulation by this lectin (Fig. 2e). L-PHA reactive *N*-glycans are also present on B cells, but L-PHA is not a B cell mitogen. Furthermore, B-cell responses to anti-IgM antibody, lipopolysaccharide and interleukin (IL)-4 plus anti-CD40 antibody were similar for cells from *Mgat5*$^{-/-}$ and *Mgat5*$^{+/+}$ mice (Fig. 2f; and data not shown). In T cells, L-PHA induces signalling common to TCR engagement, including phosphorylation of CD3ζ, Ca^{2+} mobilization, PKC-γ and Ras/mitogen-activated protein kinase (Mapk) activation[18,19]. The TCRα/β chains have seven *N*-glycans in total, and some are branched, complex-type structures with L-PHA reactivity[20,21]. These data indicate that Mgat5-modified glycans are present on glycoproteins of the TCR complex and are required for L-PHA mitogenesis.

When bound to major histocompatibility complex (MHC)/peptide, TCRs cluster with an inherent affinity greater than unligated TCRs, and the stability of these clusters is critical for intracellular signalling[22]. However, the density of TCRs measured at the site of T cell–APC (antigen-presenting cell) contact is only marginally increased relative to the remaining cell surface, leaving most of the TCRs unengaged by MHC/peptide[4]. It is possible that ligand-induced TCR clustering in the plane of the membrane may be increased in the absence of Mgat5-modified glycans, thus lowering *Mgat5*$^{-/-}$ T-cell activation thresholds. Therefore, to visualize TCR re-organization in response to an antigen-presenting surface, we coated polystyrene beads with anti-CD3ε antibody and incubated them with purified *ex vivo* T cells. After 10 min of contact, TCRs in *Mgat5*$^{-/-}$cells were markedly more concentrated at the bead surface compared with *Mgat5*$^{+/+}$cells (Fig. 3a, b). TCRs on wild-type cells could not be induced to cluster to the same extent as *Mgat5*$^{-/-}$ cells, even with longer incubations (20 min) or using anti-CD3ε plus

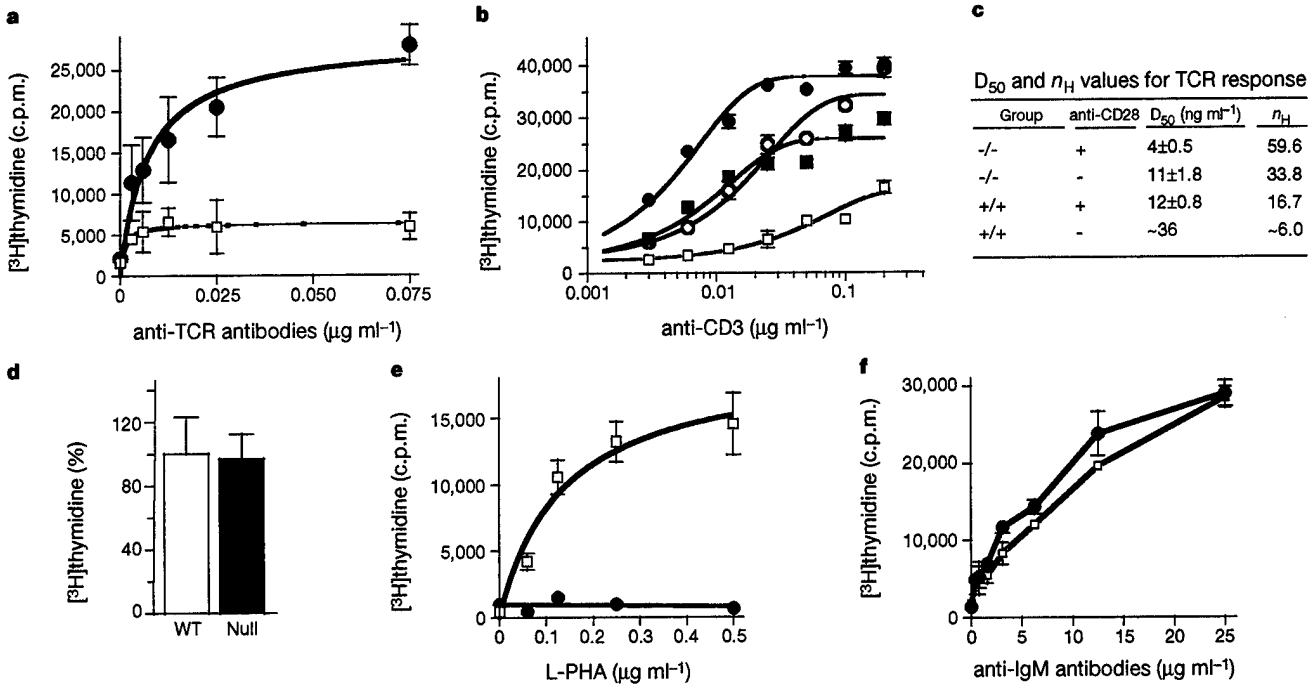

Figure 2 *Mgat5*$^{-/-}$ T cells are hypersensitive to TCR agonists. **a**, Spleen cells were cultured with anti TCRα/β antibodies for 48 h. Filled circles, *Mgat5*$^{-/-}$; open squares, *Mgat5*$^{+/+}$. **b**, Purified T cells from spleen were stimulated for 48 h with anti-CD3ε antibody in the absence (open circles and squares) or presence (filled squares and circles) of anti-CD28 antibody. *Mgat5*$^{-/-}$ and *Mgat5*$^{+/+}$ cells are indicated by circles and squares, respectively. **c**, The Hill slope (n_H) of the sigmodal curve is calculated using $Y = x^{n_H}/(k^{n_H} + x^{n_H})$. **d**, Stimulation of splenic T cells with TPA plus ionomycin for 48 h. **e**, Stimulation of splenic T cells from *Mgat5*$^{-/-}$ (filled circles) and *Mgat5*$^{+/+}$ (open squares) mice with L-PHA. **f**; Stimulation of splenic B cells from *Mgat5*$^{-/-}$ (filled circles) and *Mgat5*$^{+/+}$ (open squares) mice with anti-IgM antibody for 48 h. The means ± standard deviation of triplicate determinations are used.

anti-CD28-coated beads (data not shown). Actin microfilaments were more concentrated at the bead contact site in *Mgat5*$^{-/-}$ cells, and overlapped more extensively with TCRs in the merged images compared with *Mgat5*$^{+/+}$ T cells (Fig. 3a, b). TCRs are internalized after productive TCR clustering[1], and this was significantly greater in *Mgat5*$^{-/-}$ compared with *Mgat5*$^{+/+}$ cells (Fig. 3c, solid lines). Intracellular signalling mediated by TPA treatment induces TCR internalization but at similar rates in *Mgat5*$^{-/-}$ and *Mgat5*$^{+/+}$ cells (Fig. 3c, dotted lines). Microfilament reorganization was more rapid in Mgat5-deficient T cells after soluble anti-CD3ε antibody stimulation (Fig. 3d). Akt/protein kinase B (PKB) phosphorylation is dependent on phosphoinositide 3-OH kinase activity, which stimulates Rac/CDC42 GTPases and actin filament reorganization[23]. Phosphorylated Akt/PKB showed a greater fold increase in *Mgat5*$^{-/-}$ compared with *Mgat5*$^{+/+}$ T cells (Fig. 3d). Mobilization of intracellular Ca^{2+} after stimulation with soluble anti-CD3ε antibody was enhanced in the absence of Mgat5-modified glycans (Fig. 3e). Tyrosine phosphorylation of multiple proteins was increased and persisted longer in *Mgat5*$^{-/-}$ T cells exposed to anti-CD3ε antibody coated beads. (Fig. 3e). Immunoprecipitation of Zap-70 revealed increased phosphorylation in *Mgat5*$^{-/-}$cells 1–5 min after stimulation. Zap-70 kinase binds to dual phosphorylated immunoreceptor tyrosine-based activation motif domains of CD3ζ, and association of the latter with Zap70 was increased in *Mgat5*$^{-/-}$ compared with *Mgat5*$^{+/+}$ T cells (Fig. 3g). Thus, the Mgat5 deficiency enhanced ligand-dependent TCR aggregation, and

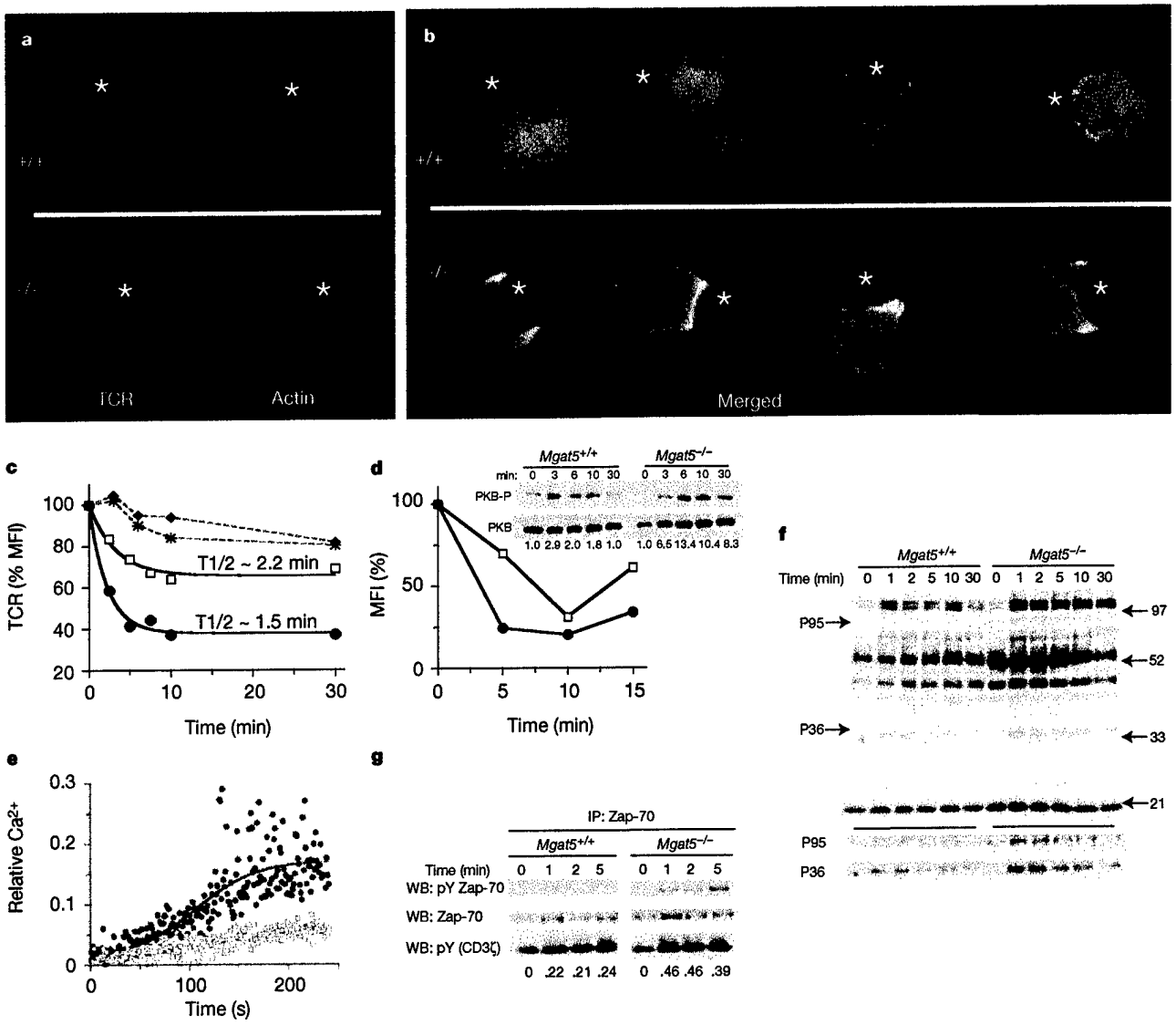

Figure 3 TCR clustering, actin re-organization and signalling in T cells from *Mgat5*$^{-/-}$ and *Mgat5*$^{+/+}$ mice. **a**, TCR and actin microfilament distribution in T cells stimulated by anti-CD3ε-coated beads. **b**, Merged images of *Mgat5*$^{-/-}$ and *Mgat5*$^{+/+}$ cells. Clustering was observed in 5 of 6 and 0 of 6 randomly photographed cells, respectively. **c**, TCR internalization by FACS analysis using FITC-anti-TCRα/β antibodies to measure cell-surface TCRs after addition of anti-CD3ε antibody. Changes in MFI with time are shown. T cells from *Mgat5*$^{-/-}$ (filled circles and squares) or *Mgat5*$^{+/+}$ (open squares and asterisks) mice were treated with anti-CD3ε antibody (filled circles (*Mgat5*$^{-/-}$) and open squares (*Mgat5*$^{+/+}$)); or with TPA (filled squares (*Mgat5*$^{-/-}$) and asterisks (*Mgat5*$^{+/+}$)). Similar results were obtained when the stimulation and detection roles of anti-TCRα/β and anti-CD3 were reversed. **d**, Actin polymer content in T cells from *Mgat5*$^{-/-}$ (filled circles), or *Mgat5*$^{+/+}$ (open squares) mice after stimulation with anti-CD3ε antibody, measured by FACS. Western blot for phospho-Akt/PKB in T-cell lysates after addition of anti-CDε antibody is shown (top). The values below are fold increase in PKB-P normalized to PKB protein. **e**, Ca^{2+} mobilization in purified T cells from *Mgat5*$^{-/-}$ (filled circles), and *Mgat5*$^{+/+}$ (open squares) mice stimulated with anti-CD3ε antibody. **f**, Western blot with anti-phosphotyrosine antibody detecting phosphorylated proteins in T-cell lysates after incubation with anti-CD3ε antibody-coated beads. A longer exposure was used to show bands (arrowheads at left) migrating as p95 and p36 shown below. Arrows at the right indicate the positions of molecular mass markers. **g**, immunoprecipitation of Zap-70 and western blotting for phosphotyrosine (pY) to detect Zap-70 and CD3ζ (values below are CD3ζ ratio P23/P21).

consequently, signal transduction and microfilament re-organization.

The larger size of Mgat5-modified glycans may limit the geometry and spacing of TCR clusters in the plane of the membrane[24]. Alternatively, Mgat5-modified glycans may bind cell-surface galectins, which restrict TCR mobility and thereby antigen-induced TCR clustering. The galectins are a widely expressed family of mammalian lectins defined as *N*-acetyllactosamine-binding proteins. The poly *N*-acetyllactosamine sequences preferentially added to Mgat5-modified glycans[6] enhance the affinity for galectin binding (Fig. 1a). Galectins bind to lactosamine and lactose with dissociation constants in the 10^{-4} M range[7,8], an affinity comparable to MHC/peptide-induced oligomerization of TCRs in solution[22]. Therefore, the avidity of a multivalent galectin–Mgat5 glycoprotein lattice at the cell surface may be sufficient to restrict TCR clustering. To probe for the presence of galectin–glycoprotein interactions, wild-type *ex vivo* T cells were preincubated with various disaccharides for 20 min before a 10 min stimulation with anti-CD3ε antibody-coated beads. Preincubation with lactose increased TCR clustering at the bead interface and reduced TCR density elsewhere on the cells (Fig. 4c), which is similar to the behaviour of untreated *Mgat5*$^{-/-}$ T cells (Fig. 3a, b). TCR clustering was not altered by preincubation with the control disaccharide sucrose (Fig. 4b). Lactosamine and lactose both enhanced protein phosphorylation induced by anti-CD3ε antibody-coated beads, but sucrose and maltose had no effect (Fig. 4d; and data not shown). Lactose did not enhance signalling in *Mgat5*$^{-/-}$T cells (data not shown).

Galectin-3 was detected on the surface of naïve T cells by labelling with sulphosuccinimidobiotin, capture with streptavidin beads and western blotting with anti-galectin-3 antibodies (Fig. 4e). Chemical crosslinking of the cell surface to stabilize complexes followed by western blotting of galectin-3 immunoprecipitates showed that galectin-3 is associated with TCR complex proteins. This interaction was disrupted by either Mgat5 deficiency or incubating wild-type T cells with 2 mM lactose (Fig. 4e). Taken together, the data demonstrate that a multivalent cell-surface galectin–glycoprotein lattice limits TCR clustering in response to agonist, the avidity of which is dependent on Mgat5-modified glycans (Fig. 4f). The full complement of glycoproteins and lectins present in the T-cell lattice remains unknown, but at a minimum includes galectin-3 and the TCR complex. Exogenously added galectin-1 binds CD2, CD3, CD4, CD7, CD43 and CD45, and these proteins may also participate in the lattice[25]. Indeed, exogenous galectin-1 modulates T-cell activation *in vitro*[9,25], antagonizes TCR signalling[26], and when injected into mice it suppresses the pathology of EAE[27].

The gene replacement vector used to produce our Mgat5-deficient mice contained the reporter gene *LacZ*, replacing the first exon, which was expressed with the same tissue specificity as *Mgat5* transcript[16]. Both the *LacZ* expression and cell-surface Mgat5-modified glycans in *Mgat5*$^{-/-}$ and *Mgat5*$^{+/+}$ T cells, respectively,

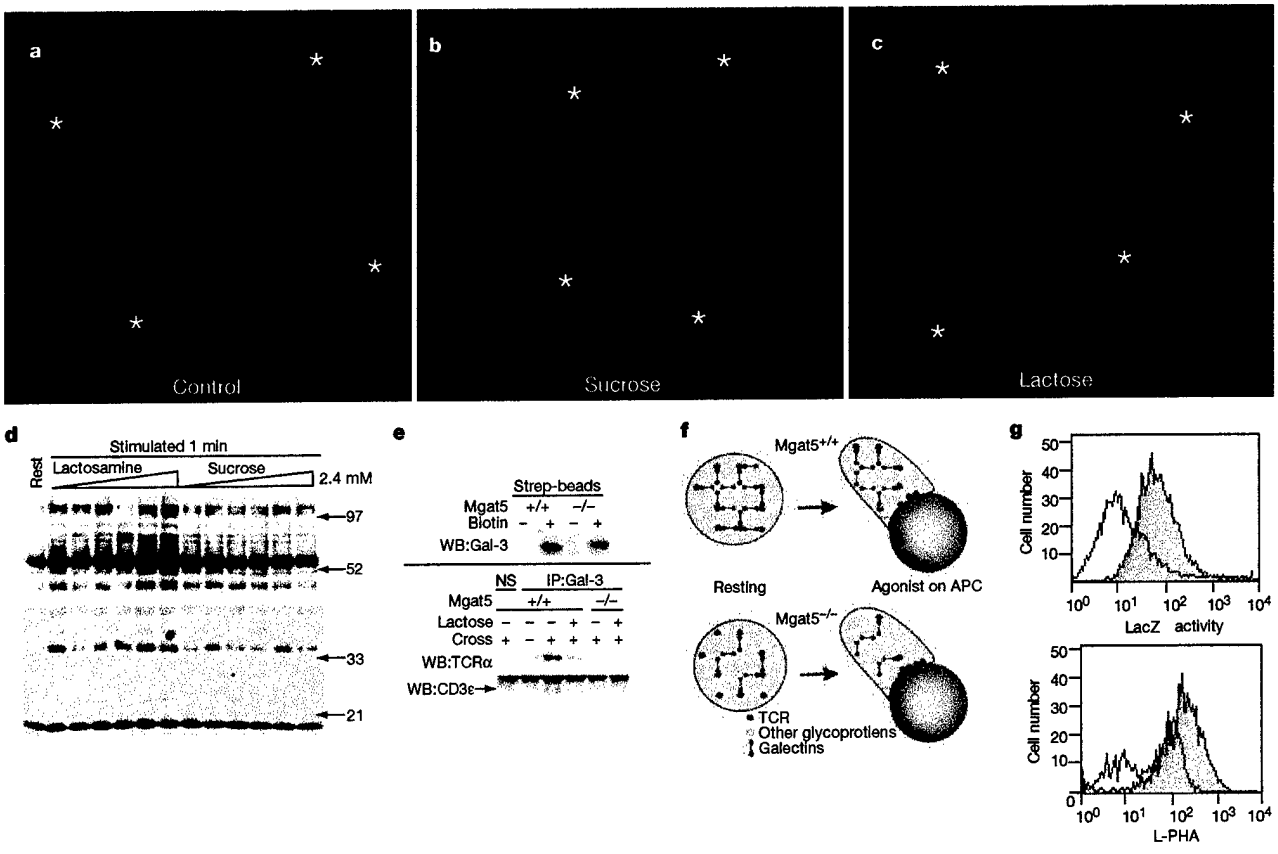

Figure 4 Lactose stimulates TCR aggregation and signalling in *Mgat5*$^{+/+}$ mice. **a–c**, Purified T cells preincubated for 20 min with buffer (**a**), 2 mM sucrose (**b**), or 2 mM lactose (**c**), then stimulated with anti-CD3ε antibody-coated beads for 10 min and stained for TCRs. Enhanced TCR clustering was observed in 0 of 10, 1 of 10 and 9 of 10 cases, respectively. **d**, *Mgat5*$^{+/+}$ T cells incubated with increasing concentrations of disaccharide (1/3 serial dilution from 2.4 mM) and stimulated for 1 min with anti-CD3ε antibody-coated beads compared for phosphotyrosine. Arrows at the right indicate the positions of molecular mass markers. A longer exposure of the lower molecular weight portion of the blot is shown. **e**, Galectin-3 detected by surface labelling with NHS-biotin on T cells. Association of galectin-3 with CD3ε and TCRα chain, and its disruption by Mgat5 deficiency and lactose is shown (bottom). **f**, Model showing restricted mobility of TCRs by interaction with a galectin–glycoprotein network, which is stronger in Mgat5-expressing cells. **g**, Upper panel shows *LacZ* activity in untreated (white) and anti-CD3 and anti-CD28-stimulated (grey) T cells from *Mgat5*$^{-/-}$ mice. Lower panel, L-PHA-binding to *Mgat5*$^{+/+}$ T lymphocytes either untreated (white) or stimulated with anti-CD3 and anti-CD28 for 48 h (grey).

increased 48 h after stimulation, demonstrating regulation of Mgat5 by transcriptional means (Fig. 4g). This suggests that Mgat5 enzyme activity and glycan production are limiting in resting T cells, and with stimulation, increases in Mgat5-modified glycans and galectins may dampen TCR sensitivity to antigen. Negative feedback by Mgat5-modified glycans on TCR sensitivity is delayed as it requires Mgat5 gene expression, which is dependent on T-cell activation status, and only indirectly on antigen concentrations. This form of slow-negative regulation governed by steady-state activity of the system is a key feature of robust and adaptive biochemical pathways[28], and Mgat5-modified glycans may contribute this feature to T-cell regulation.

It has been estimated that sustained clustering of roughly 8,000 TCRs is required for T-cell activation[2], but other molecular interactions clearly alter this threshold. With CD28 co-stimulation, only about 1,500 TCRs are required[2]. Co-signalling through CD28 decreases the extent of TCR clustering needed for activation predominantly by recruiting protein kinase-enriched GM1 ganglioside rafts to the site of TCR engagement, thereby amplifying signalling[3,5]. We show that Mgat5 deficiency increases the number of TCRs recruited to the antigen-presenting surface, thereby reducing the requirement for CD28 co-receptor engagement. This may lead to T-cell activation in the absence of CD28 co-signalling, failure of anergy and loss of immune tolerance. *CD28*$^{-/-}$ mice are resistant to induction of EAE by low dose MBP, whereas *Mgat5*$^{-/-}$ mice are hypersensitive, but both mutants develop clinical signs of EAE comparable to wild-type littermates with high doses of MBP[29]. In this regard, CD28 and Mgat5 function as opposing regulators of T-cell activation thresholds and susceptibility to autoimmune disease. Mgat5-dependent glycosylation limits agonist-induced TCR clustering by sequestering receptors in a cell-surface galectin–glycoprotein lattice. However, the glycosylation deficiency in *Mgat5*$^{-/-}$ mice affects other pathways and cell types that may also contribute to the observed autoimmunity. Indeed, Mgat5-modified glycans also reduce clusters of fibronectin receptors, causing accelerated focal adhesion turnover in fibroblasts and tumour cells; a functionality that may affect leukocyte motility[16]. Finally, glycosylation of Notch receptor by Fringe, a fucose-specific β1,3-GlcNAc-transferase, provides another example of regulation by differential receptor glycosylation[30]. In a broad context, our results suggest a general mechanism for the regulation of receptor clustering through differential glycosylation and interaction with cell-surface lectins. □

Methods

Delayed-type hypersnsitivity skin reaction

To induce DTH, 100 μl of 5% (w/v) 4-ethoxymethilene-2-phenyl-2-oxazolin-5-one (oxazolone) (Sigma) in ethanol/acetone (3:1, v/v) was injected epicutaneously to the shaved backs of the 129 mice. Four days after sensitization, 25 μl of 1% (w/v) oxazolone was applied on each side of the right ear, and the left ear received 25 μl of olive oil/acetone on each side. Ear swelling was measured with a micrometer at 24 h intervals for the next 5 d, and swelling was reported as the difference between the ear thickness of the right minus the left ears.

EAE model

Mice (129) 8–12 weeks of age were injected subcutaneously with 100 μl of rabbit MBP (Sigma) emulsified 1:1 with complete Freund's adjuvant at three different total doses (25, 100 and 500 μg per mouse). Mice were observed from day 5 to day 50, and observations were blinded with respect to the genotype until day 36. For lower doses of 25 and 50 μg, half the total was injected on day 0 in the right flank and the other half on day 7 in the left flank. The high dose of 500 μg per mouse was injected all on day 0 at the base of the tail, and 500 ng of pertussis toxin was injected through the tail vein on day 0 and day 2.

T-cell proliferation

Naïve T-cells were purified from spleens of 8–12-week-old mice by negative selection using $CD3^+$ T-cell purification columns. T-cell proliferation was measured by culturing cells for 48 h in RPMI, 10% FCS, 10^{-5}M 2-mercaptoethanol in the presence of one or more of the following soluble antibodies: hamster anti-mouse CD3ε (clone 2C11; Cedarlane), hamster anti-mouse TCRα/β (clone H59.72; Pharmingen) or 0.5 μg ml^{-1} anti-mouse CD 28 (Pharmingen). TPA (10 ng ml^{-1}) and ionomycin (0.5 μg ml^{-1}) were also used to stimulate cells. We added 2 μCi of [^{3}H]thymidine for the last 20 h of incubation, and we collected cells on fibreglass filters and measured radioactivity in a β-counter.

TCR clustering

Six-micro polystyrene beads (Polysciences) in PBS were coated with hamster anti-mouse CD3ε antibody (Clone 2C11; Cederlane) at 2 μg ml^{-1} antibody followed by coating with 200 μg ml^{-1} bovine serum albumin. To measure TCR clustering, 5×10^4 T cells were incubated with 2.5×10^5 anti-CD3ε antibody-coated beads in 100 μl RPMI 1640 + 10% FCS at 37 °C for 10 min, placed on poly-L-lysine-coated cover slips. The cells were fixed with 10% formalin, stained with 2 μg ml^{-1} fluorescein isothiocyanate (FITC)-labelled anti-TCRα/β antibody (Pharmingen), solubilized with 0.2% Triton X-100, labelled with rhodamine-phalloidin and Hoechst, and then visualized by deconvolution microscopy. To measure TCR internalization, purified splenic T cells stimulated with either 0.1 μg ml^{-1} anti-CD3 antibody or with 10 ng ml^{-1} TPA for varying lengths of time were collected and stained with FITC–anti-TCRα/β. TPA concentrations were not limiting as 10, 50 and 100 ng ml^{-1} produced similar internalization and cell activation results. To measure actin reorganization, purified splenic T cells stimulated with 0.1 μg ml^{-1} anti-CD3 for varying lengths of time were fixed with 4% paraformaldehyde for 10 min, washed with PBS and stained with rhodamine-phalloidin, and mean fluorescence intensity (MFI) was determined by FACS.

TCR signalling

T cells (10^6) and anti-CD3ε antibody-coated beads (5×10^6at 0.4 ug ml^{-1} antibody) in 100 μl RPMI 1640 were pelleted, incubated at 37 °C for various times, then solublized with ice-cold 50 mM Tris pH 7.2, 300 mM NaCl, 0.5% Triton X-100, protease inhibitor cocktail (Boehringer Mannheim) and 2 mM orthovanadate. Zap-70 was immunoprecipitated by incubating whole-cell lysates with rabbit polyclonal anti-Zap-70 agarose conjugate (Santa Cruz) overnight at 4 °C, followed by one wash with lysis buffer and three washes with PBS. Western blotting was done with whole-cell lysates or immunoprecipitates separated on SDS–polyacrylamide gel electrophoresis gels under reducing conditions, transferred electrophoretically to polyvinylidene difluoride membranes, and immunoblotted with antibodies to Akt/PKB (NEB), phospho-Akt/PKB (NEB), phosphotyrosine (clone 4G10; Upstate Biotechnology), Zap-70 (clone Zap-70-6F7; Zymed), TCRα (polyclonal; Santa cruz) and rabbit anti-galectin-3 (a gift from A. Raz, University of Michigan). Cell-surface proteins were biotinylated using sulphosuccinimidobiotin (NHS-biotin) for 30 min, PBS pH 8.0. Cells were lysed and labelled protein was captured on streptavidin-agarose beads. To crosslink surface proteins on purified naïve T cells, the homobifunctional crosslinker dithio-bis(sulphosuccinimydylpropionate) (DTSSP) was used at 0.1 mg ml^{-1} with 10^6 cell per ml in PBS pH 8.0 for 10 min at 20 °C. T cells were preincubated for 20 min with or without 2 mM lactose, and reacted with DTSSP in the presence of the same. Aliquots of cell lysate were immunoprecipitated with rabbit anti-galectin-3 antibody or non-immune rabbit serum (NS), separated on reducing SDS–PAGE, and western blotted for CD3ε and TCRα chain. The band above CD3ε is a cross-reactivity of secondary antibody with light-chain.

To measure Ca^{2+} mobilization, purified T cells were loaded with 10 μM AM ester of Fluo-3 (Molecular Probes), washed and stimulated with 10 μg ml^{-1} anti-CD3ε antibody at 37 °C. We took emission at 525 nm using a spectrofluorimeter with excitation at 488 nm. Data is plotted as a fraction of the Ca^{2+} mobilized by addition of 2 μg ml^{-1} of ionomycin. *LacZ* activity in *Mgat5*$^{-/-}$ T cells was detected by loading cells with fluorescein-di-β-D-galactopyranoside (FDG) (Molecular Probes) at 10 °C, and allowing the reaction to proceed for 30 min. The reaction was stopped by the addition of 1 mM phenyl-β-thiogalactoside.

Received 11 September; accepted 29 November 2000.

1. Valitutti, S., Mulle, S., Cella, M., Padovan, E. & Lanzavecchia, A. Serial triggering of many T-cell receptors by a few peptide–MHC complexes. *Nature* **375**, 148–151 (1995).
2. Viola, A. & Lanzavecchia, A. T cell activation determined by T cell receptor number and tunable thresholds. *Science* **273**, 104–106 (1996).
3. Viola, A., Schroeder, S., Sakakibara, Y. & Lanzavecchia, A. T lymphocyte costimulation mediated by reorganization of membrane microdomains. *Science* **283**, 680–682 (1999).
4. Monks, C. R., Feiberg, B. A., Kupfer, H., Sciaky, N. & Kupfer, A. Three-dimensional segregation of supramolecular activation clusters in T cells. *Nature* **395**, 82–86 (1998).
5. Wulfing, C. & Davis, M. M. A receptor/cytoskeletal movement triggered by costimulation during T cell activation. *Science* **282**, 2266–2269 (1998).
6. Cummings, R. D. & Kornfeld, S. The distribution of repeating Gal β1-4GlcNAc β1-3 sequences in asparagine-linked oligosaccharides of the mouse lymphoma cell line BW5147 and PHAR 2.1. *J. Biol. Chem.* **259**, 6253–6260 (1984).
7. Sato, S. & Hughes, R. C. Binding specificity of a baby hamster kidney lectin for H type I and II chains, polylactosamine glycans, and appropriately glycosylated forms of laminin and fibronectin. *J. Biol. Chem.* **267**, 6983–6990 (1992).
8. Knibbs, R. N., Agrwal, N., Wang, J. L. & Goldstein, I. J. Carbohydrate-binding protein 35. II. Analysis of the interaction of the recombinant polypeptide with saccharides. *J. Biol. Chem.* **268**, 14940–14947 (1993).
9. Perillo, N. L., Pace, K. E., Seilhamer, J. J. & Baum, L. G. Apoptosis of T cells mediated by galectin-1. *Nature* **378**, 736–739 (1995).
10. Vespa, G. N. *et al.* Galectin-1 specifically modulates TCR signals to enhance TCR apoptosis but inhibit IL-2 production and proliferation. *J. Immunol.* **162**, 799–806 (1999).
11. Karsan, A. *et al.* Leukocyte Adhesion Deficiency Type II is a generalized defect of de novo GDP-fucose biosynthesis. Endothelial cell fucosylation is not required for neutrophil rolling on human non-lymphoid endothelium. *J. Clin. Invest.* **101**, 2438–2445 (1998).
12. Ellies, L. G. *et al.* Core 2 oligosaccharide biosynthesis distinguishes between selectin ligands essential for leukocyte homing and inflammation. *Immunity* **9**, 881–890 (1998).
13. Priatel, J. J. *et al.* The ST3Gal-I sialyltransferase controls CD8+ T lymphocyte homeostasis by modulating O-glycan biosynthesis. *Immunity* **12**, 273–283 (2000).

14. Wall, K. A., Pierce, J. D. & Elbein, A. D. Inhibitors of glycoprotein processing alter T-cell proliferative responses to antigen and to interleukin 2. *Proc. Natl Acad. Sci. USA* **85**, 5644–5648 (1988).
15. Cummings, R. D., Trowbridge, I. S. & Kornfeld, S. A mouse lymphoma cell line resistant to the leukoagglutinating lectin from *Phaseolus vulgaris* is deficient in UDP-GlcNAc:α-D-mannoside β1,6 N-acetylglucosaminyltransferase. *J. Biol. Chem.* **257**, 13421–13427 (1982).
16. Granovsky, M. *et al.* Suppression of tumor growth and metastasis in Mgat5-deficient mice. *Nature Med.* **6**, 306–312 (2000).
17. Lafaille, J. J., Nagashima, K., Katsuki, M. & Tonegawa, S. High incidence of spontaneous autoimmune encephalomyelitis in immunodeficient anti-myelin basic protein T cell receptor transgenic mice. *Cell* **78**, 399–408 (1994).
18. Downward, J., Graves, J. D., Warne, P. H., Rayter, S. & Cantrell, D. A. Stimulation of $p21^{ras}$ upon T-cell activation. *Nature* **346**, 719–723 (1990).
19. Trevillyan, J. M., Lu, Y. L., Atluru, D., Phillips, C. A. & Bjorndahl, J. M. Differential inhibition of T cell receptor signal transduction and early activation events by a selective inhibitor of protein-tyrosine kinase. *J. Immunol.* **145**, 3223–3230 (1990).
20. Wang, J. *et al.* Atomic structure of an αβ T cell receptor (TCR) heterodimer in complex with an anti-TCR fab fragment derived from a mitogenic antibody. *EMBO J.* **17**, 10–26 (1998).
21. Hubbard, S. C., Kranz, D. M., Longmore, G. D., Sitkovsky, M. V. & Eisen, H. N. Glycosylation of the T-cell antigen-specific receptor and its potential role in lectin-mediated cytotoxicity. *Proc. Natl Acad. Sci. USA* **83**, 1852–1856 (1986).
22. Reich, Z. *et al.* Ligand-specific oligomerization of T-cell receptor molecules. *Nature* **387**, 617–620 (1997).
23. Reif, K. & Cantrell, D. A. Networking Rho family GTPases in lymphocytes. *Immunity* **8**, 395–401, (1998).
24. Rudd, P. M. *et al.* Roles for glycosylation of cell surface receptors involved in cellular immune recognition. *J. Mol. Biol.* **293**, 351–366 (1999).
25. Pace, K. E., Lee, C., Stewart, P. L. & Baum, L. G. Restricted receptor segregation into membrane microdomains occurs on human T cells during apoptosis induced by galectin-1. *J. Immunol.* **163**, 3801–3811 (1999).
26. Chung, C. D., Patel, V. P., Moran, M., Lewis, L. A. & Carrie Miceli, M. Galectin-1 induces partial TCR zeta-chain phosphorylation and antagonizes processive TCR signal transduction. *J. Immunol.* **165**, 3722–3729 (2000).
27. Offner, H. *et al.* Recombinant human beta-galactoside binding lectin suppresses clinical and histological signs of experimental autoimmune encephalomyelitis. *J. Neuroimmunol.* **28**, 177–184 (1990).
28. Barkal, N. & Leibler, S. Robustness in simple biochemical networks. *Nature* **387**, 913–917 (1997).
29. Oliveira-dos-Santos, A. J. *et al.* CD28 costimulation is crucial for the development of spontaneous autoimmune encephalomyelitis. *J. Immunol.* **162**, 4490–4495 (1999).
30. Moloney, D. J. *et al.* Fringe is a glycosyltransferase that modifies Notch. *Nature* **406**, 369–375 (2000).

Acknowledgements

We thank S. Kulkarni and J. Tsang for technical assistance. This research was supported by grants from NCI of Canada, the Mizutani Foundation, the National Science and Engineering Research Council of Canada, and GlycoDesign, Toronto.

Correspondence and requests for materials should be addressed to J.W.D. (e-mail: dennis@mshri.on.ca).

Crystal structure of photosystem II from *Synechococcus elongatus* at 3.8 Å resolution

Athina Zouni*, Horst-Tobias Witt*, Jan Kern*, Petra Fromme*, Norbert Krauß†, Wolfram Saenger†, Peter Orth†

**Max-Volmer-Institut für Biophysikalische Chemie und Biochemie, Technische Universität Berlin, Straße des 17, Juni 135, D-10623, Berlin, Germany*
† Institut für Chemie, Kristallographie, Freie Universität Berlin, Takustrasse 6, D-14195 Berlin, Germany

Oxygenic photosynthesis is the principal energy converter on earth. It is driven by photosystems I and II, two large protein–cofactor complexes located in the thylakoid membrane and acting in series. In photosystem II, water is oxidized; this event provides the overall process with the necessary electrons and protons, and the atmosphere with oxygen. To date, structural information on the architecture of the complex has been provided by electron microscopy of intact, active photosystem II at 15–30 Å resolution[1], and by electron crystallography on two-dimensional crystals of D1-D2-CP47 photosystem II fragments without water oxidizing activity at 8 Å resolution[2]. Here we describe the X-ray structure of photosystem II on the basis of crystals fully active in water oxidation[3]. The structure shows how protein subunits and cofactors are spatially organized. The larger subunits are assigned and the locations and orientations of the cofactors are defined. We also provide new information on the position, size and shape of the manganese cluster, which catalyzes water oxidation.

Conversion of light to chemical energy at photosystem II (PSII) is associated with charge separation across the thylakoid membrane (for review see ref. 4). It is initiated by ejection of an electron from the excited primary donor P680, a chlorophyll *a* located towards the luminal side of the membrane at the heart of the PSII reaction centre that is formed by protein subunits D1 and D2. When the cationic radical $P680^{\bullet+}$ is formed, the electron moves by means of a pheophytin to the electron stabilizing acceptor Q_A, a plastoquinone that is tightly bound at the stromal side of subunit D2. After each of four successive charge separating steps that are light induced, $P680^{\bullet+}$ abstracts one electron from a manganese cluster (generally assumed to contain four manganese ions) by means of the redox-active tyrosine residue Tyr_Z. In turn, the four positive charges accumulated in the manganese cluster oxidize two water molecules, coupled with the release of one O_2 and four H^+. In the first two charge separations, $Q_A^{\bullet}$ doubly reduces one mobile molecule Q_B docked to the binding site B on D1. After uptake of two protons, Q_BH_2 is released into the plastoquinone pool that is embedded in the membrane, and replaced by a new Q_B from the pool for another round of reduction and release.

We isolated PSII from the thermophilic cyanobacterium *Synechococcus elongatus* in the form of homodimers as shown by electron microscopy (E. J. Boekema, unpublished observations). With these preparations, three-dimensional crystals were grown[5] that are suitable for X-ray analysis (see Methods). According to SDS–polyacrylamide gel electrophoresis and mass-spectrometry (MALDI-TOF) (data not shown), this PSII is composed of at least 17 subunits[6] of which 14 are located within the photosynthetic membrane: the reaction centre proteins D1 (PsbA) and D2 (PsbD); the chlorophyll-containing inner-antenna subunits CP43 (PsbC) and CP47 (PsbB); α- and β-subunits of cytochrome *b*-559 (PsbE and PsbF); and the smaller subunits PsbH, PsbI, PsbJ, PsbK, PsbL, PsbM, PsbN and PsbX. The membrane-extrinsic cytochrome *c*-550

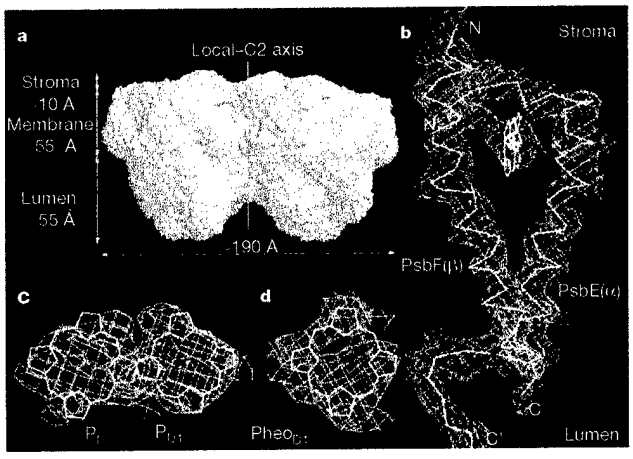

Figure 1 Electron densities of PSII after density modification and their interpretation. **a**, Surface of PSII homodimer drawn from the averaging mask generated during density modification. View direction along the membrane plane; the position of local-C2 rotation axis, is shown. **b**, Cytochrome (Cyt) *b*-559 heterodimer with electron densities contoured at 1.2 σ (r.m.s. deviation above the mean electron density) for protein and haem group, and at 4.0 σ for Fe^{2+}. The termini of the α-helices are labelled N, C for the α-subunit, and N′, C′ for the β-subunit. **c**, Head groups of P680 chlorophyll (Chl) *a* P_{D1} and P_{D2} with view perpendicular to their planes. Mg^{2+} are depicted as red spheres. **d**, Head group of pheophytin $Pheo_{D1}$.

Revised Aug 1, 2000
Current Opin. in Structr Biology.

Genetic defects in *N*-glycosylation and cellular diversity in mammals

James W. Dennis*, Charles E. Warren, Michael Demetriou and Maria Granovsky

Samuel Lunenfeld Research Institute
Mount Sinai Hospital
600 University Ave. R988
Toronto, Ontario,
Canada M5G 1X5
& *Department of Molecular & Medical Genetics
University of Toronto
Phone: 416-586-8233
FAX: 416-586-8588
Email: Dennis@mshri.on.ca

Abstract

Glycoproteins in mammalian cells are modified with complex-type Asn-linked glycans of variable chain lengths and composition. Observations with mutations in glycosyltransferase genes suggest that *N*-glycan structures regulate T cell receptor clustering and thereby sensitivity to agonists. We argue that the heterogeneity inherent in N-glycosylation contributes to cellular diversity, and thereby adaptability in the immune system.

Abbreviations:

TCR	T cell receptor
CDG	congenital disorders of glycosylation
PyMT	polyomavirus middle T oncogene
APC	antigen presenting cells
CRD	carbohydrate-recognition domains
peptide-MHC	antigenic peptide bound to major histocompatibility complex

Introduction:

N- and *O*- linked glycans are found on both cell surface and secreted proteins, many of which control proliferation and cell fate decisions in animals. Tissue-specificity expression of glycosyltransferases is a significant factor controlling the glycan profiles observed in differentiated cells (1). In addition, many glycosyltransferases compete for acceptor intermediates causing bifurcations of the pathways and additional structural complexity (2). Heterogeneity at specific Asn-X-Ser/Thr sites on individual glycoproteins is very common, and diversifies the molecular population into glycoforms. The protein environment of each Asn-X-Ser/Thr influences access by processing enzymes, and inefficiencies in this process result in only a fraction of *N*-glycans receiving certain substitutions. As a result, each Asn-X-Ser/Thr site of a glycoprotein is commonly populated by a set of biosynthetically related *N*-glycan structures.

The specific activity of particular functional properties can vary between individual glycoforms and thus the potency of a glycoprotein is actually the weighted-average of the specific activities of the glycoform population. For example, the peptide hormones lutropin and erythropoietin are produced with structurally diverse glycans, and the discrete glycoforms differ in affinity for hepatic lectins thereby determining serum half-lives and potency *in vivo* (3; 4). By balancing the proportions of glycoforms with different serum half-life, the potency and kinetics of cytokine response can be modified or adapted to extrinsic conditions. In a similar manner, variation in receptor glycosylation has the potential to modify their physical associations in the membrane, and thereby the ligand occupancy thresholds for signal transduction. The terminal portions of mature *N*-glycans are generally not bound to the glycoprotein on which they reside. This leaves them free to bind to multivalent lectins at the cell surface. Different receptor glycoforms should have a range of affinities for these cell surface lectins and thereby regulate ligand-dependent receptor movement as previously suggested by Feizi and Childs (5). Receptor systems that form highly cooperative macromolecular clusters in response to agonists such as T cell receptor (TCR) and cell adhesion receptors appear to be sensitive to glycoform variation. Herein we discuss phenotypes associated with mutations in

enzymes of the glycosylation pathways, and their implications concerning the molecular functions of cell surface N-glycans.

Congenital disorders of glycosylation

The first stage of protein *N*-glycosylation, conserved from yeast to man, is synthesis of $Glc_3Man_9GlcNAc_2$-PP-dolichol and transfer of the oligosaccharide to proteins in the ER. Five type I congenital disorders of glycosylation (CDG) are known, each with a characteristic enzymatic defects in $Glc_3Man_9GlcNAc_2$-pp-dolichol biosynthesis or transfer to Asn. Infants with these defects share clinical features, which include developmental delay, multiple organ abnormalities, and severe neurologic dysfunction (6)(7)*. These deficiencies result in partial failure to glycosylate proteins at the usual Asn-X-Ser/Thr sites with oligosaccharides. A complete deficit of *N*-glycosylation is expected to be incompatible with life, as inhibition of oligosaccharyltransferase by tunicamycin is toxic to yeast and mammalian cells. $G_1Man_{7-9}GlcNAc_2$ on newly synthesized glycoproteins binds calnexin, calreticulin, and ER α-glucosyltransferase. The latter acts as a sensor of glycoprotein conformations, and combined with the action of α-glucosidase II, a deglucosylation-reglucosylation cycle continues and retains the glycoprotein until proper folding occurs fulfilling a function analogous to that of chaperones (8; 9)*.

CDG type I patients display a remarkable variability in clinical phenotypes, even for example between patients that have the same mutant alleles of phosphomannomutase gene *PMM2* (6). The genetic background of each patient can presumably influence the expressivity of a phenotype in a complex manner. The chaperone function of $Glc_1Man_{7-9}GlcNAc_2$ may vary depending on polymorphism in the underlying polypeptides, and this could influence the clinical phenotype. "Silent" polymorphisms are common in the population, and may be innocuous until revealed by a "molecular stress", such as the under-glycosylated state present in CDG patients. This is analogous to the inactivation of the chaperone Hsp90 in *Drosophila*, which revealed the accumulated genetic variation between strain backgrounds as morphological mutations (10)**. In an evolutionary context, environmental stresses that compromise the buffering capacity of protein chaperones including those that rely on *N*-glycans may reveal a reservoir of genetic diversity for rapid adaptation (10)**.

Complex-type N-glycans in embryogenesis and immune regulation.

The GlcNAc-TI gene, *Mgat1* is ubiquitously expressed and required in the biosynthesis of all hybrid and complex-type *N*-glycans (figure 1A). *Mgat1*$^{-/-}$ mouse embryos die at around E9.5 with failures of neural tube formation, vascularization and determination of left-right body plan asymmetry (11; 12). Maternal sources of Mgat1 enzyme and *N*-glycan products are present in the pre-E6 day embryos and may support development until E9.5, after which complex-type glycans are largely depleted (13). In chimeric embryos, *Mgat1*$^{-/-}$ cells contributed to various tissues with the exception of lung bronchial epithelium (14). Consistent with this observation, the *Mgat1*$^{-/-}$ embryos display a severe failure to organize bronchial epithelium. As Mgat1 mutant Chinese hamster ovary cells grow normally in culture, the *in vivo* data on failure of *Mgat1*$^{-/-}$ embryos supports the notion that complex-type *N*-glycans mediate cell-cell interactions in the animal. Growth conditions for Mgat1 deficient cells are not limiting in culture, or presumably in most tissues of the Mgat1 chimeric mice. However, when growth conditions are limiting, as in low-serum cultures, mutant tumor cells with defects in either GlcNAc-TV (Mgat5) or Golgi UDP-Gal transporter were observed to grow at reduced rates and displayed an increased dependency on autocrine growth factors (15).

These studies suggested that complex-type *N*-glycans on certain cell surface receptors affect their sensitivity to growth factors and/or adhesion signals. Indeed, some glycostransferases mutant mice may be sensitized, and although they appear normal at birth, phenotypes can be revealed by stresses and aging, as well as by moving the mutations onto different inbred strain backgrounds. In this regard, mammary tumor growth and metastases induced by a polyomavirus middle T (PyMT) mice was significantly reduced in *Mgat5*$^{-/-}$ mice on the 129/sv x FVB background. The PyMT protein is an intracellular docking protein that transforms cells by activating the Ras signaling pathways as well as phosphatidylinositol 3-kinase and protein kinase B (PKB/Akt). These latter enzymes are downstream effects of focal adhesion signaling, which appears to be impaired in *Mgat5*$^{-/-}$ tumor cells and embryonic fibroblasts. Mgat5 modified glycans are present on integrin $\alpha5\beta1$, and their depletion may stabilize substratum attachment and thereby impair PyMT signaling and tumor growth in *Mgat5*$^{-/-}$ mice (16)**. A cancer phenotype has also been revealed in *Mgat3*$^{-/-}$ mice by treating

them with a carcinogen. Diethylnitrosamine-induced hepatocarcinomas progress more slowly in *Mgat3*$^{-/-}$ mice compared to wild type littermates. Further analysis of the mice indicated that an autocrine factor which dependent upon Mgat3 and expressed in a tissue other than liver promotes tumor growth (17)*.

In the absence of GlcNAc-TII (Mgat2), complex-type *N*-glycans are replaced by hybrid-type glycans (figure 1A). Inactivating mis-sense mutations have been identified in *Mgat2* that reduce enzyme activity by >95% in two CDG type IIa patients (18). This is a rare autosomal recessive disorder characterized by multi-systemic involvement and severe impairment of the nervous system. *Mgat2*$^{-/-}$ mice are runted, and die at variable times after birth with multiple organ defects (Chui and Marth, personal communication) further evidence that complex-type *N*-glycans are required for normal embryogenesis.

Mutations disrupting fewer glycan structures generally result in viable animals with tissue-restricted or conditional phenotypes. These include mutations that affect late steps in the processing pathway or enzymes with functional redundancies. Immune phenotypes have been detected in a number of viable glycosyltransferase mutant mice, indicating a particular sensitivity of immune cells to changes in glycosylation. ST6Gal mutants are impaired in B cell proliferation (19) and ST3GalI mutant mice display a loss of peripheral CD8+ T cells in the absence of stimulation (20). The E-, P- and L- selectins and their ligands control leukocyte traffic. Mutations in glycosyltransferases that produce selectin ligands disrupt trafficking but differ qualitatively, presumable due to the details of glycan structure and their tissue distribution. These include Fuc-TIV, Fuc-TVII (21), the O-linked core 2 GlcNAc-T(L) branching enzyme(22) and a β3GlcNAc-T that extends core1 O-glycans with 6-sulfo sialyl LeX (23). Mice deficient in the N-linked processing enzymes α-mannosidase II (24)* and Mgat5 both develop autoimmune kidney disease with age (25)**.

Mgat5-modified glycans regulate T cell receptor sensitivity to antigen

Mgat5$^{-/-}$ mice lack detectable GlcNAcβ1,6Manα1,6 branched *N*-glycan products and are born healthy from CD1 outbred and 129/sv inbreed mouse strains (16). However, small litter sizes and higher perinatal mortality has been observed with *Mgat5* mutation on the PLJ mouse background, a hyper-immune mouse strain (Pawling, Demetriou et al. unpublished observations). *Mgat5*$^{-/-}$ mice displayed an age-dependent autoimmune

disease characterized by glomerulonephritis (25). T cell dependent immune reactions were exaggerated in *Mgat5*$^{-/-}$ mice, and T cells in culture were hypersensitive to TCR agonists. Delayed type hypersensitivity was more severe, and susceptibility to experimental autoimmune encephalomyelitis, a model for human multiple sclerosis, was greater in mutant mice. In contrast, *Mgat5*$^{-/-}$ B cells responded normally to a variety of stimuli, indicating a degree of cell-type specificity to the defect.

TCR are recruited into "immune synapses" by peptide-MHC on antigen presenting cells (APC), where a threshold number of receptors is required to sustain intracellular signaling and trigger entry into S phase (26). This rate-limiting event of sustained TCR clustering was enhanced in *Mgat5*$^{-/-}$ cells (Figure 2). TCR-dependent tyrosine phosphorylation, actin microfilament reorganization, and Ca^{++} mobilization were enhanced in *Mgat5*$^{-/-}$ T cells, but intracellular signaling down-stream of TCR induced by phorbol ester was unchanged. These results indicate that T cell hypersensitivity in *Mgat5*$^{-/-}$ cells is due to change at the cell surface (25). In quiescent T cells, Mgat5 gene expression is low, and rate-limits for cell surface β1,6GlcNAc branched *N*-glycan levels. Both the enzyme activity and glycans increase following activation (25). Therefore, Mgat5 glycans are both regulated during T cell maturation, and a determinant of TCR sensitivity to agonists.

Some glycoproteins recycle through the endocytic pathway and back to the cell surface, but this does not involve remodeling of *N*-glycan branching. As such, d*e novo* synthesis and turnover of cell surface glycoproteins presumably takes hours compared to antigen-induced TCR signaling, which occurs in minutes after TCR engagement by agonits. Therefore, increasing Mgat5 gene expression and Mgat5-modified glycans at the cell surface is a form of slow negative feedback governed over time by the steady-state activity of signaling downstream of TCR. This type of delayed negative has been observed in other pathways, and provides a mechanism to adjust or tune receptor sensitivity to match ambient conditions. (27). T cells in different tissue environments may alter Mgat5-modified glycans levels, thereby adapt TCR sensitivity and response threshold.

Lectin-glycan interactions modulate lymphocyte receptor signalling

The TCRα and β chains together have 7 *N*-glycans, and CD3 γ and δ each have one chain. Glycosylation is necessary for assembly of these peptides into a mature TCR complex. The *N*-glycans protrude ~30Å from the protein surface and a fraction of these glycans appear by their positive L-PHA reactivity, to be β1,6GlcNAc-branched complex-type structures (28), which are preferentially substituted with poly *N*-acetyllactosamine (29). Electron density of the chitobiose core ($GlcNAc_2$) of *N*-glycans is often observed in high-resolution X-ray structures (30)*. However, density for distal *N*-glycan sequences is generally not visible in X-ray structures, consistent with their mobility and lack of order in the crystal. Biantennary complex-type *N*-glycans have been modeled onto TCR complex. Based on their size and positions, it has been proposed that *N*-glycans may limit non-specific receptor aggregation and thereby spurious T cell activation (30). The glycans may also align the geometry for TCR binding towards peptide-MHC on the APC (30)*.

We recently reported that glycoproteins of the TCR complex bind to galectins at the cell surface, which impede TCR clustering in response to agonist (25). The galectin family is conserved in metazoans, and features either one or two carbohydrate-recognition domains (CRD). Galectins-1 and –3 have one CRD and form homodimers with CRDs spaced ~50Å apart and oriented in opposing directions(31), a feature ideally suited for cross linking glycoproteins with multiple glycans (32) (Figure 2). Treatment of wild type T cells with lactose or lactosamine to dissociate the galectins from their endogenous ligands enhanced TCR clustering and tyrosine phosphorylation in response to agonist, in essence creating a phenocopy of *Mgat5*$^{-/-}$ (25). Furthermore, cell surface galectin-3 was found physically associated with TCR complex, an interaction enhanced by expression of Mgat5 glycans. Monomeric affinities of galectins for lactosamine and lactose are in the 10^{-3}M range (33), which is comparable to peptide-MHC-induced oligermerization of TCR measured in solution, and lower than TCR affinity for peptide-MHC to form an immune synapse (26). Poly *N*-acetyllactosamine, a slightly higher affinity ligand (10^{-4}M) for galectin-3 (33), is preferentially added to Mgat5-modified glycans (29)(Figure 1A). Therefore Mgat5 glycans on the TCR complex and other

glycoproteins appear to form a multivalent lattice held together by galectins, that slow the migration of the TCR into clusters at immune synapse (Figure 2A,C).

There are at least 10 mammalian galectins with overlapping expression patterns. Galectin-1 or –3 deficient mice are healthy, but have not yet been examined for T cell or stress-related phenotypes (34). Galectin-3 and the TCR complex are present in the T cell lattice, and galectin-1 has been reported to bind CD2, CD3, CD4, CD7, CD43 and CD45 on T cells (35), but other components of the lattice remain to be defined. Exogenous galectin-3 and galectin-1 modulate T cell activation *in vitro* (35), antagonize TCR signaling (36)**, and when injected into mice, galectin-1 can suppress autoimmune disease (37). Galectin-3 expressed at the cell surface in cancer cells increases tumor growth, invasion, and metastasis (38)*, possibly by enhancing turnover of integrin-substratum contacts and thereby focal adhesions.

Siglecs are sialic acid binding lectins implicated in lymphoid and myeloid cell functions. CD22 (siglec-2) binds ST6Gal products (SAα2,6Galβ) in *cis* on the B cell surface. Unlike galectins, CD22 is a transmembrane protein with a cytosolic domain that is phosphorylated and recruits Grb2, Shc, SHP1 and SHIP, causing reduced B cell receptor signaling (39). B cells of CD22 deficient mice are hypersensitive to antigen stimulation. However, ST6Gal deficient mice display impaired B cell proliferation, attenuated antibody production, and although cell surface CD22 is present, it is unbound to ligand (40). This suggests that recruitment of CD22 into B cell receptor signaling complexes is inhibited by SAα2,6Galβ. Therefore the SAα2,6Galβ appears to be a negative regulator of a negative regulator (ie. CD22), and loss of the former allows CD22 to dampen the B cell response. Such a possible scenario is depicted by the model in Figure 1B (and represented by the right panel). ST6Gal activity (41), and CD22 occupancy with sialic acid is regulated with B cell activation (42). Similar to Mgat5 regulation in T cells, this suggests that the signaling threshold for B cell receptor may be regulated by differential sialylation, which controls the availability of CD22.

Structural diversity of glycans increases functional diversity

Individual cells typically show small variances for many molecular parameters that together, confer a gaussian spectrum of responsiveness in the cell population. Protein glycosylation machinery appears to be designed to increase molecular heterogeneity, and

presumably in some instances, functional diversity within cell populations. While different receptor glycoforms may vary only slightly in their affinities for lectins and signal transduction, exponential amplification of lymphocyte clones can convert small differences into large systemic events (43). T cell clones undergo multiple rounds of cell division once triggered by peptide-MHC binding above a threshold affinity. Once this stochastic event occurs, strong positive feedback by cytokines creates a highly cooperative and sustained expansion of cells. Many other interactions between cells regulate the balance of Th1/Th2 helper T cells, development of memory T cells, and cessation of the response. The immune system appears to be particularly sensitive to small functional difference at the cellular level, which with a certain probability, are amplified and impact host physiology.

Sustained clustering of ~8000 TCRs concentrates protein kinases and docking proteins on the inner surface of the membrane at sufficient levels to trigger T cell activation(44). However, co-receptor CD28 binding to CD80 on the APC enhances the recruitment of intracellular signaling molecules, and thereby reducing by 5 fold the number of TCRs required for activation (45; 46). The Mgat5 deficiency sensitizes this system still further, displaying a lower TCR agonist threshold independent of CD28 co-stimulation (25) (Figure 1C). In addition, the apparent Hill coefficient (n_H) was increased in Mgat5 deficiency cells, and this represents the synchrony of the responding cell population in this experiment. Although each T cell responds individually in a switch-like manner, the inherent heterogeneity between cells for *N*-glycans and other factors such as CD28 levels tend to reduce the synchrony or apparent cooperativity of the responding cell population (Figure 1C) (47). The Mgat5 mutation eliminates a subset of *N*-glycans, reducing molecular heterogeneity in the remaining *N*-glycans, and presumably the heterogeneity of the glycoprotein-galectin lattice (Figure 1B). Mgat5 glycans are present on $\alpha 1\beta 5$ integrin, and in a similar manner Mgat5$^{-/-}$ cells show increased cooperativity for adhesion (16) while over-expression of Mgat5 has the opposite effect on response to substratum (48) (Figure 1D).

Coffey has argued convincingly that complex biological systems such as the immune system might be modeled using non-linear dynamics and chaos theory, beginning with simple rules of interaction governing the behavior of cells in the system

(49)**. The calculated outcomes over time appear unpredictable, but they are confined to a bounded set, and are highly dependent on basal conditions, and particularly the genetic background. Living systems evolve towards the boundary of order and chaos where the system has maximum fitness. Loss of diversity in the lymphocyte population affects the probability of infection and autoimmune diseases as suggested by many gene knockout experiments in mice. For example, CD28 deficient mice are more resistant to autoimmune disease but more sensitive to certain pathogens. Resistance to infections and development of cancer verses the maintenance of self-tolerance are in some respects opposing objectives of the immune system, and balanced for overall fitness. Mgat5 deficient mice are hypersensitivity to autoimmune disease but display reduced breast cancer progression in a transgenic oncogene model of cancer (16).

Structurally diverse glycans are present on many receptors that may also be regulated by interactions with lectins as discussed here for TCR, integrins and CD22. It would appear that incremental effects of glycoform variation on highly cooperative events such as TCR clustering at the molecular level, and lymphocyte activation at the cell population level, can set thresholds for systemic events such as susceptibility to auoimmune disease. Although further evidence is needed to support our hypothesis, it is possible that the structural diversity of glycans may be an important feature of adaptability and fitness designed to regulate receptor thresholds and variances of cellular responses to extrinsic stimuli.

Acknowledgments

Research supported by grants to JWD from, CIHR, NSERC, US Army Breast Cancer Program, GlycoDesign Inc., Toronto.

Figure Legends:

Figure 1

(A) Scheme of the *N*-glycan biosynthesis pathway. Abbreviations used are oligosaccharyltransferase, OT; the α-glucosidases, GI, GII; the β-*N*-acetylglycosaminyltransferases, TI, TII, TIII, TIV, TV, T(i); the α1,2mannosidases, MI, α1,3/6mannosidases MII, MIII; β1,4-galactosyltransferases (Gal-T), α-

fucosyltransferases (Fuc-T), α-sialyltransferases (SaT), sulfotransferase (SO4-T). The circled numbers 1 to x represent biosynthetically related subsets of glycans labeled here only to illustrate the model shown below. **(B)** Hypothetical model to represent variability or plasticity within the T cell population. For each T cell, entry into S phase is a switch-like event that initiates activation and several rounds of cell division. Each black line represents individual cells or groups of cells that share a similar *N*-glycan structural profile. The weighted-contributions of glycoforms (k1-kx) contribute to the cell phenotype ($Z_{i,}$), and in particularly the response to agonist. The mean response to agonists is the sum of responses for the population over all Zi. The dashed lines depict the influence of Mgat5 glycans. The mean response has a D_{50} and Hill slope as depicted by the colored line for wt, Mgat5 deficient and Mgat5 over-expression. The latter panel may also apply to ST6gal deficient cells. Note the variance in the cell population is largest for wt and reduced in the mutants **(C)** Purified T cells were stimulated at low density for 48h with increasing concentrations of soluble anti-TCR antibody in the presence or absence of anti-CD28 antibody. (Data from ref (25). The genotypes and stimulation in each curve is indicated in the table on the right. **(D)** Adhesion of *Mgat5*$^{-/-}$ (solid) and wild type (open) leukocytes to increasing concentrations of fibronectin.

Figure 2

(A) A model depicting restricted mobility of TCR by interaction with a galectin - glycoprotein network, and increased of avidity in Mgat5-expressing cells. The ball represents an antigen presenting cell or anti- TCR antibody-coated bead (*). **(B)** Merged images of *Mgat5*$^{-/-}$ and *Mgat5*$^{+/+}$ cells showing TCR (green) and actin microfilament (red) distribution in T cells stimulated by anti-CD3ε coated beads (*). (From (25). **(C)** Scheme of galectin cross-linked of glycoproteins by binding to Mgat5-modified glycan structures.

Reference List

1. Paulson, J.C. and Colley, K.J. Glycosyltransferases: Structure, localization, and control of cell type-specific glycosylation. J.Biol.Chem., *264*: 17615-17618, 1989.

2. Schachter, H. Biosynthetic controls that determine the branching and microheterogeneity of protein-bound oligosaccharides. Biochem.Cell Biol., *64*: 163-181, 1986.

3. Fiete, D., Srivastava, V., Hindsgaul, O., and Baenziger, J.U. A hepatic reticuloendothelial cell receptor specific for SO_4-4GalNAcβ1,4GlcNAcβ1,Manα that mediates rapid clearance of lutropin. Cell, *67*: 1103-1110, 1991.

4. Takeuchi, M. and Kobata, A. Structures and functional roles of the sugar chains of human erythropoietins. Glycobiology, *1*: 337-346, 1991.

5. Feizi, T. and Childs, R.A. Carbohydrates as antigenic determinants of glycoproteins. Biochem.J., *245*: 1-11, 1987.

6. Carchon, H., Van Schaftingen, E., Matthijs, G., and Jaeken, J. Carbohydrate-deficient glycoprotein syndrome type IA (phosphomannomutase-deficiency). Biochim.Biophys.Acta, *1455*: 155-165, 1999.

7. Freeze, H.H. and Aebi, M. Molecular basis of carbohydrate-deficient glycoprotein syndromes type I with normal phosphomannomutase activity. Biochim.Biophys.Acta, *1455*: 167-781, 1999.

8. Helenius, A. and Aebi, M. Intracellular functions of N-linked glycans. Science, *291*: 2364-2369, 2001.

9. Parodi, A.J. Protein glucosylation and its role in protein folding. Ann.Rev.Biochem., *69*: 69-93, 2000.

10. Rutherford, S.L. and Lindquist, S. Hsp90 as a capacitor for morphological evolution. Nature, *396*: 336-342, 1998.

11. Metzler, M., Gertz, A., Sarkar, M., Schachter, H., Schrader, J.W., and Marth, J.D. Complex asparagine-linked oligosaccharides are required for morphogenic events during post-implantation development. EMBO J., *13*: 2056-2065, 1994.

12. Ioffe, E. and Stanley, P. Mice lacking N-acetylglucosaminyltransferase I activity die at mid-gestation, revealing an essential role for complex or hybrid N-linked carbohydrates. Proc.Natl.Acad.Sci.USA, *91*: 728-732, 1994.

13. Ioffe, E., Liu, Y., and Stanley, P. Complex N-glycans in Mgat1 null preimplantation embryos arise from maternal Mgat1 RNA. Glycobiology, *7*: 913-919, 1997.

14. Ioffe, E., Liu, Y., and Stanley, P. Essential role for complex *N*-glycans in forming an organized layer of bronchial epithelium. Proc.Natl.Acad.Sci.USA, *93*: 11041-11046, 1996.

15. VanderElst, I. and Dennis, J.W. N-linked oligosaccharide processing and autocrine-stimulation of tumor cell proliferation. Exp.Cell Res., *192*: 612-613, 1991.

16. Granovsky, M., Fata, J., Pawling, J., Muller, W.J., Khokha, R., and Dennis, J.W. Suppression of tumor growth and metastasis in Mgat5-deficient mice. Nature Med., *6*: 306-312, 2000.

17. Yang, X., Bhaumik, M., Bhattacharyya, R., Gong, S., Rogler, C.E., and Stanley, P. New evidence for an extra-hepatic role of *N*-acetylglucosaminyltransferase III in the progression of diethylnitrosamine-induced liver tumors in mice. Cancer Res., *6*: 3313-3319, 2000.

18. Tan, J., Dunn, J., Jaeken, J., and Schachter, H. Mutations in the MGAT2 gene controlling complex N-glycan synthesis cause carbohydrate-deficient glycoprotein syndrome type II, an autosomal recessive disease with defective brain development. Am J Hum Genet, *59*: 810-817, 1996.

19. Hennet, T., Chui, D., Paulson, J.C., and Marth, J.D. Immune regulation by the ST6Gal sialytransferase. Proc.Natl.Acad.Sci.USA, *95*: 4504-4509, 1998.

20. Priatel, J.J., Chui, D., Hiraoka, N., Simmons, C.J., Richardson, K.B., Page, D.M., Fukuda, M., Varki, N.M., and Marth, J.D. The ST3Gal-I sialyltransferase controls CD8+ T lymphocyte homeostasis by modulating O-glycan biosynthesis. Immunity, *12*: 273-283, 2000.

21. Maly, P., Thall, A.D., Petryniak, B., Rogers, C.E., Smith, P.L., Marks, R.M., Kelly, R.J., Gersten, K.M., Cheng, G., Saunders, T.L., Camper, S.A., Camphausen, R.T., Sullivan, F.X., Isogai, Y., Hindsgaul, O., von Andrian, U.H., and Lowe, J.B. The α(1,3)fucosyltransferase fuc-TVII controls leukocyte trafficking through an essential role in L-, E-, and P-selectin ligand biosynthesis. Cell, *86*: 643-653, 1996.

22. Snapp, K.R., Heitzig, C.E., Ellies, L.G., Marth, J.D., and Kansas, G.S. Differential requirements for the O-linked branching enzyme core 2 beta1-6-N-glucosaminyltransferase in biosynthesis of ligands for E-selectin and P-selectin. Blood, *97*: 3806-3811, 2001.

23. Yeh, J., Hiraoka, N., Petryniak, B., Nakayama, J., Ellies, L.G., Rabuka, D., Hindsgaul, O., Marth, J.D., Lowe, J.B., and Fukuda, M. Novel Sulfated Lymphocyte Homing Receptors and Their Control by a Core1 Extension beta1,3-N-Acetylglucosaminyltransferase. Cell, *105*: 957-969, 2001.

24. Chui, D., Sellakumar, G., Green, R., Sutton-Smith, M., McQuistan, T., Marek, K., Morris, H., Dell, A., and Marth, J. Genetic remodeling of protein glycosylation in vivo induces autoimmune disease. Proc.Natl.Acad.Sci.USA, *98*: 1142-1147, 2001.

25. Demetriou, M., Granovsky, M., Quaggin, S., and Dennis, J.W. Negative regulation of T-cell activation and autoimmunity by Mgat5 N-glycosylation. Nature, *409*: 733-739, 2001.

26. Reich Z, Boniface JJ, Lyons DS, Borochov N, Wachtel EJ, and Davis MM Ligand-specific oligomerization of T-cell receptor molecules. Nature, *387*: 617-620, 1997.

27. Alon, U., Surette, M.G., Barkai, N., and Leibler, S. **Robustness in bacterial chemotaxis**. Nature, *397*: 168-171, 1999.

28. Hubbard, S.C., Kranz, D.M., Longmore, G.D., Sitkovsky, M.V., and Eisen, H.N. Glycosylation of the T-cell antigen-specific receptor and its potential role in lectin-mediated cytotoxicity. Proc.Natl.Acad.Sci.USA, *83*: 1852-1856, 1986.

29. Cummings, R.D. and Kornfeld, S. The distribution of repeating Gal β1-4GlcNAc β1-3 sequences in asparagine-linked oligosaccharides of the mouse lymphoma cell line BW5147 and PHAR 2.1. J.Biol.Chem., *259*: 6253-6260, 1984.

30. Rudd, P.M., Wormald, M.R., Stanfield, R.L., Huang, M., Mattsson, N., Speir, J.A., DiGennaro, J.A., Fetrow, J.S., Dwek, R.A., and Wilson, I.A. Roles for glycosylation of cell surface receptors involved in cellular immune recognition. J Mol Biol, *293*: 351-366, 1999.

31. Lobsanov, Y.D., Gitt, M.A., Leffler, H., Barondes, S.H., and Rini, J.M. X-ray crystal structure of the human dimeric S-Lac lectin, L-14-II, in complex with lactose at 2.9-A resolution. J Biol Chem, *268*: 27034-27038, 1993.

32. Mandal, D.K. and Brewer, C.F. Cross-linking activity of the 14-kilodalton beta-galactoside-specific vertebrate lectin with asialofetuin: comparison with several galactose-specific plant lectins. Biochemistry, *31*: 8465-8472, 1993.

33. Sato, S. and Hughes, R.C. Binding specificity of a baby hamster kidney lectin for H type I and II chains, polylactosamine glycans, and appropriately glycosylated forms of laminin and fibronectin. J Biol Chem, *267*: 6983-6990, 1992.

34. Colnot, C., Fowlis, D., Ripoche, M.A., Bouchaert, I., and Poirier, F. Embryonic implantation in galectin 1/galectin 3 double mutant mice. Dev Dyn, *211*: 306-313, 1998.

35. Pace, K.E., Lee, C., Stewart, P.L., and Baum, L.G. Restricted receptor segregation into membrane microdomains occurs on human T cells during apoptosis induced by galectin-1. J Immunology, *163*: 3801-3811, 1999.

36. Chung, C.D., Patel, V.P., Moran, M., Lewis, L.A., and Carrie Miceli, M. Galectin-1 induces partial TCR zeta-chain phosphorylation and antagonizes processive TCR signal transduction. J Immunol, *165*: 3722-3729, 2000.

37. Offner, H., Celnik, B., Bringman, T.S., Casentini-Borocz, D., Nedwin, G.E., and Vandenbark, A.A. Recombinant human beta-galactoside binding lectin suppresses clinical and histological signs of experimental autoimmune encephalomyelitis. J Neuroimmunol, *28*: 177-184, 1990.

38. Gong, H.C., Honjo, Y., Nangia-Makker, P., Hogan, V., Mazurak, N., Bresalier, R.S., and Raz, A. The NH2 terminus of galectin-3 governs cellular compartmentalization and functions in cancer cells. Cancer Res, *59*: 6239-6245, 1999.

39. Poe, J.C., Fujimoto, M., Jansen, P.J., Miller, A.S., and Tedder, T.F. CD22 forms a quaternary complex with SHIP, Grb2, and Shc. A pathway for regulation of B lymphocyte antigen receptor-induced calcium flux. J.Biol.Chem., *275*: 17420-17427, 2000.

40. Hennet, T., Chui, D., Paulson, J.C., and Marth, J.D. Immune regulation by the ST6Gal sialytransferase. Proc.Natl.Acad.Sci.USA, *95*: 4504-4509, 1998.

41. Wuensch, S.A., Huang, R.Y., Ewing, J., Liang, X., and Lau, J.T. Murine B cell differentiation is accompanied by programmed expression of multiple novel beta-galactoside alpha2, 6-sialyltransferase mRNA forms. Glycobiology, *10*: 67-75, 2000.

42. Razi, N. and Varki, A. Masking and unmasking of the sialic acid-binding lectin activity of CD22 (Siglec-2) on B lymphocytes. Proc.Natl.Acad.Sci.USA, *95*: 4697-7474, 1998.

43. Germain, R.N. The art of the probable: system control in the adaptive immune system. Science, *293*: 240-245, 2001.

44. Viola, A. and Lanzavecchia, A. T cell activation determined by T cell receptor number and tunable thresholds. Science, *273*: 104-106, 1996.

45. Viola, A., Schroeder, S., Sakakibara, Y., and Lanzavecchia, A. T lymphocyte costimulation mediated by reorganization of membrane microdomains. Science, *283*: 680-682, 1999.

46. Wulfing, C. and Davis, M.M. A receptor/cytoskeletal movement triggered by costimulation during T cell activation. Science, *282*: 2266-2269, 1998.

47. Ferrell, J.E.Jr. and Machleder, E.M. The biochemical basis of an All-or-none cell fate switch in *Xenopus* oocytes. Science, *280*: 895-898, 1998.

48. Demetriou, M., Nabi, I.R., Coppolino, M., Dedhar, S., and Dennis, J.W. Reduced contact-inhibition and substratum adhesion in epithelial cells expressing GlcNAc-transferase V. J.Cell Biol., *130*: 383-392, 1995.

49. Coffey, D.S. Self-organization, complexity and chaos: the new biology for medicine. Nat Med, *4*: 882-885, 1998.

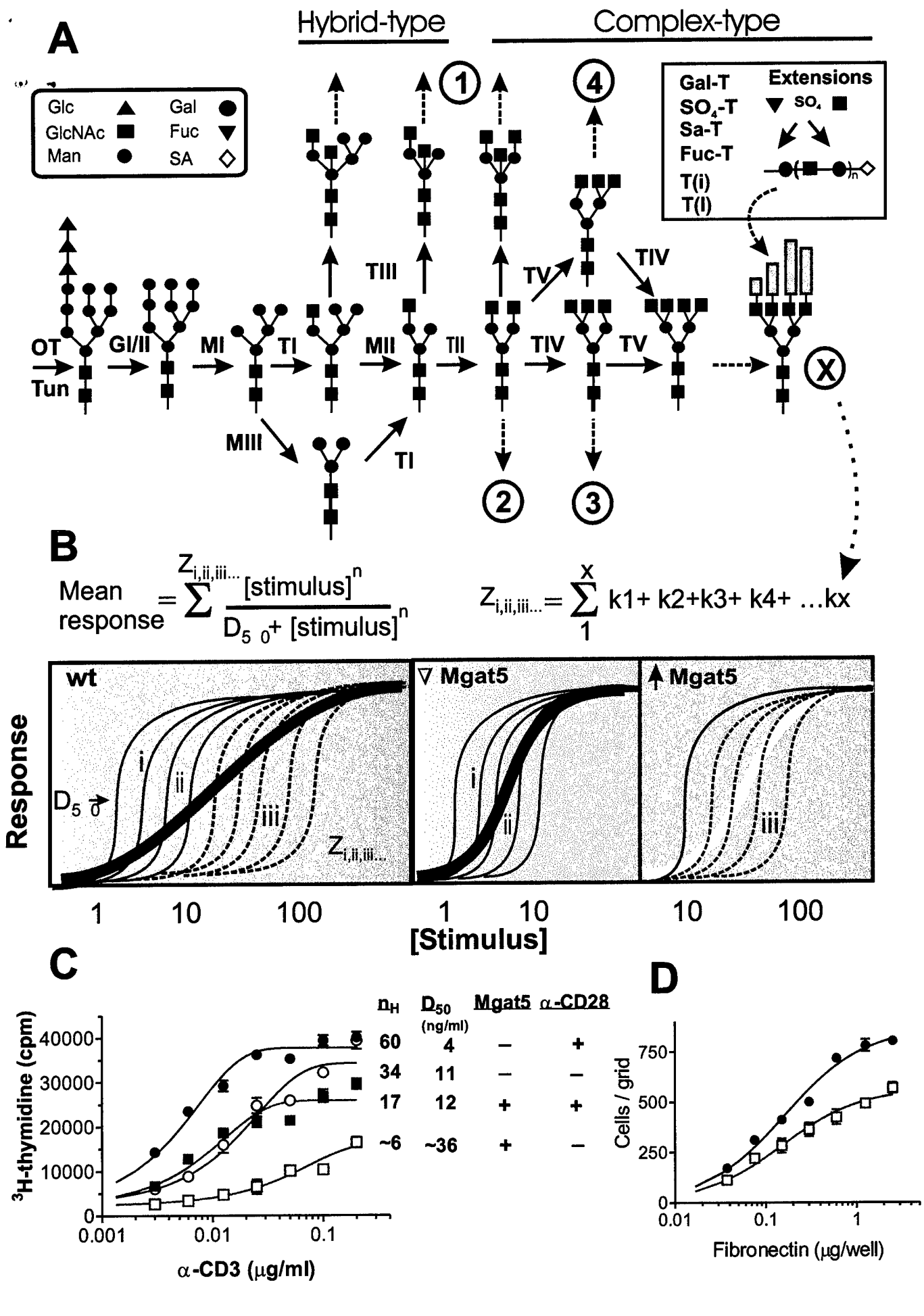
A
Hybrid-type
Complex-type
Glc
GlcNAc
Man
Gal
Fuc
SA
Gal-T
SO4-T
Sa-T
Fuc-T
T(i)
T(I)
Extensions
OT
Tun
GI/II
MI
TI
TIII
MII
TII
TV
TIV
MIII
TI
1
2
3
4
X
B
Mean response = Σ Z i,ii,iii... [stimulus]^n / D50 + [stimulus]^n
Z i,ii,iii... = Σ 1 x k1+ k2+k3+ k4+ ...kx
wt
Mgat5
Mgat5
Response
D5 0
i
ii
iii
Z i,ii,iii...
1
10
100
[Stimulus]
C
3H-thymidine (cpm)
40000
30000
20000
10000
0
0.001
0.01
0.1
α-CD3 (μg/ml)
nH
D50 (ng/ml)
Mgat5
α-CD28
60
4
–
+
34
11
–
–
17
12
+
+
~6
~36
+
–
D
Cells / grid
750
500
250
0
0.01
0.1
1
Fibronectin (μg/well)

Figure 1

Figure 2

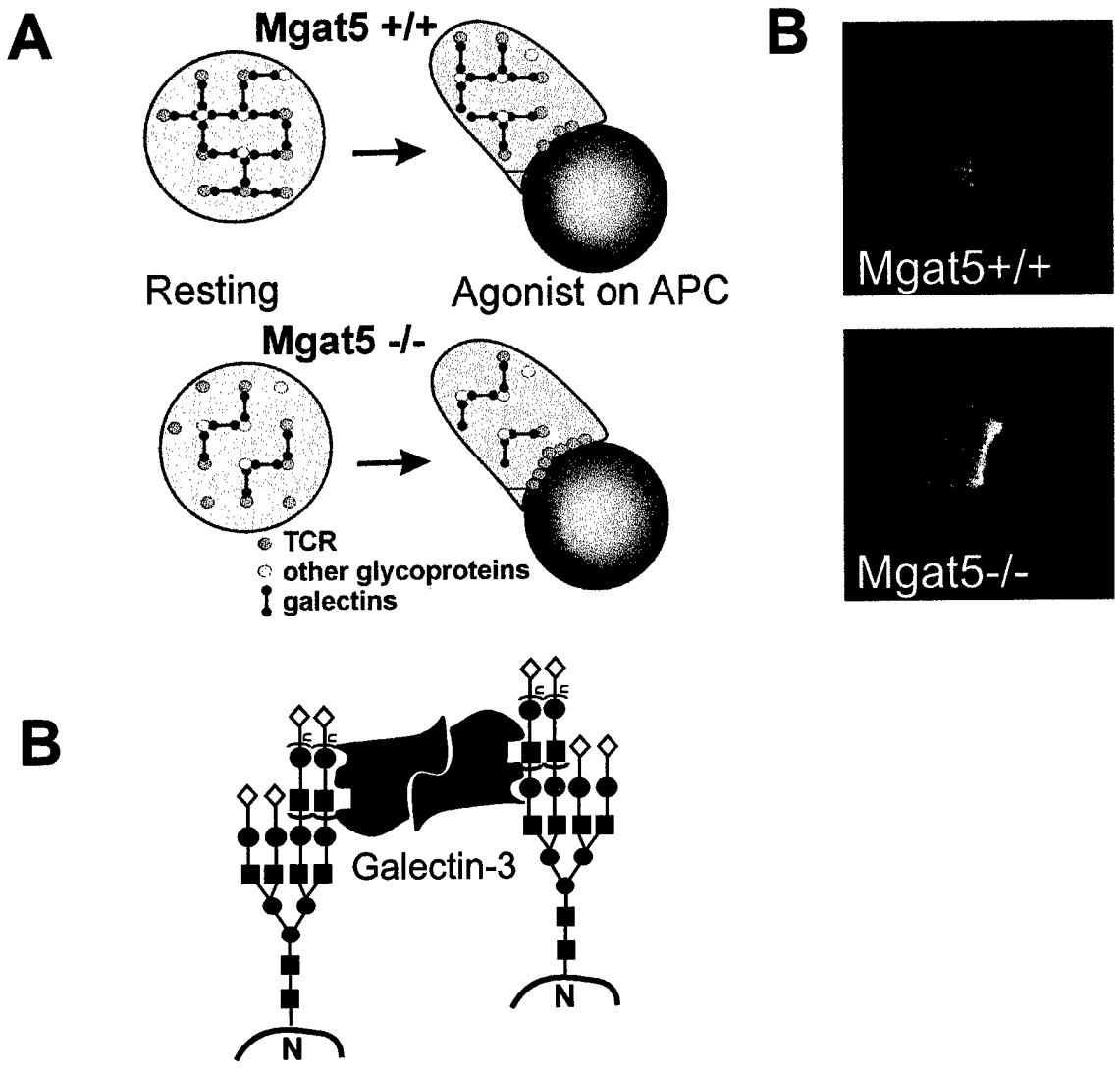
A
Mgat5 +/+
Resting
Agonist on APC
Mgat5 -/-
TCR
other glycoproteins
galectins
B
Mgat5+/+
Mgat5-/-
B
Galectin-3
N
N